

## Article

# From Fresh Itabirites and Carbonates to Weathered Iron Ore: Mineral Composition, Density and Porosity of Different Fresh and Altered Rocks from the Quadrilátero Ferrífero, Brazil

Diniz Ribeiro <sup>1,\*</sup>, Israel Moraes <sup>1</sup>, Rogerio Kwitko-Ribeiro <sup>2</sup>, Deivid Braga <sup>1</sup>, Carlos Spier <sup>3</sup>  and Pedro Santos <sup>4</sup>

<sup>1</sup> Vale S.A., Iron Resource Management, Escritório de Águas Claras, Nova Lima, MG 34.006-200, Brazil; israel.moraes@vale.com (I.M.); Deivid.braga@vale.com (D.B.)

<sup>2</sup> Vale S.A., Mineral Technology, Centro de Desenvolvimento Mineral, Santa Luzia, MG 33.040-900, Brazil; rogerio.kwitko@vale.com

<sup>3</sup> School of Earth and Environmental Sciences, The University of Queensland, Saint Lucia, QLD 4072, Australia; c.spier@uq.edu.au

<sup>4</sup> Independent Consultant, Itabira, MG 35.900-360, Brazil; pedroapoloniodossantos@gmail.com

\* Correspondence: diniz.ribeiro@vale.com

**Abstract:** The weathering of Paleoproterozoic itabirites (metamorphic-banded iron formations) and dolomites from the Cauê and Gandarela Formations in the Quadrilátero Ferrífero (QF), Brazil, produces supergene iron ore with different mineralogical, chemical, and physical properties. In this work, we present a methodology to assess the changes in chemical and physical features of those rocks during weathering, via quantitative analyses of mineral assemblages. These mineral assemblages were calculated from chemical analyses of fresh and weathered samples collected from drill holes drilled in different iron ore deposits in the QF. In general, the number of mineral species found in fresh or/and weathered itabirite is restricted, which helps the quantification of the mass and volumes of minerals by normative calculation in a large dataset of drilling and channel samples. The calculation of the bulk density takes into consideration, besides the mineral phases, the voids and free water in the altered rock matrix. This study shows that the estimated porosity in supergene ore varies from 0% to 20%, for compact materials, and from 15% to 55% for friable rocks, indicating an important process of rock matrix dissolution during the weathering of itabirites. In this process, MgO, CaO, and FeO are leached out from carbonates, talc, and amphiboles. Magnetite is oxidized to hematite, releasing Fe<sup>2+</sup>, which is oxidized and precipitates as Fe-hydroxide. There is a concentration of Fe<sub>2</sub>O<sub>3</sub>, MnO, Al<sub>2</sub>O<sub>3</sub>, and SiO<sub>2</sub> in the supergene ore (saprolite) by residual enrichment or recrystallization of hematite, goethite, quartz, manganese oxides, and kaolinite. A calculation of weathering effects on the original protoliths allowed for the establishment of a correlation between different types of fresh itabirites and their corresponding weathered materials. The calculation was carried out in several steps, to account for changes in porosity and masses and has taken into consideration differences in the mineralogical composition of the protolith. Within the weathered zones, a strong link is observed between the existence of collapse on the topographic surface and the presence of supergene ore underneath. The partial to total dissolution of quartz and carbonates from the protolith itabirite results in very porous materials and leads to gravitational collapses.



**Citation:** Ribeiro, D.; Moraes, I.; Kwitko-Ribeiro, R.; Braga, D.; Spier, C.; Santos, P. From Fresh Itabirites and Carbonates to Weathered Iron Ore: Mineral Composition, Density and Porosity of Different Fresh and Altered Rocks from the Quadrilátero Ferrífero, Brazil. *Minerals* **2021**, *11*, 29. <https://doi.org/10.3390/min11010029>

Received: 24 August 2020

Accepted: 15 October 2020

Published: 29 December 2020

**Publisher's Note:** MDPI stays neutral with regard to jurisdictional claims in published maps and institutional affiliations.



**Copyright:** © 2020 by the authors. Licensee MDPI, Basel, Switzerland. This article is an open access article distributed under the terms and conditions of the Creative Commons Attribution (CC BY) license (<https://creativecommons.org/licenses/by/4.0/>).

## 1. Introduction

The increasing demand in the iron ore market in the last decades has intensified the mining companies' interest for the marginal, low-Fe grade (<45 wt. % Fe) iron ore deposits. As a consequence, exploration programs were accelerated, aiming to increase mineral resources and improve the geological knowledge of itabirites (metamorphosed

banded iron formations (BIFs), [1]), with focus on non-weathered itabirites. In 2010, Vale started a project entitled “Geology of Compact Itabirites in the Quadrilátero Ferrífero (QF)” aiming to investigate the continuity of the layers of itabirites in-depth through deep drilling. The following iron ore deposits were studied: Conceição/Minas do Meio (CCE/MMI), Pico/Sapecado (PIC/SAP), Galinheiro (GAL), Abóboras (ABO), Jangada (JGD), Gongo Soco (GSO), Capitão do Mato (CMT), Alegria (ALG), Fábrica Nova (FNO), Fábrica (SEG/JPE), Fazendão (FAZ), Capanema (CAP) and Timbopeba (TBO). In total, 19,273.90 m were drilled in 32 drill holes from 12 deposits, with an approximate average of 600 m per drill hole (Figure 1).

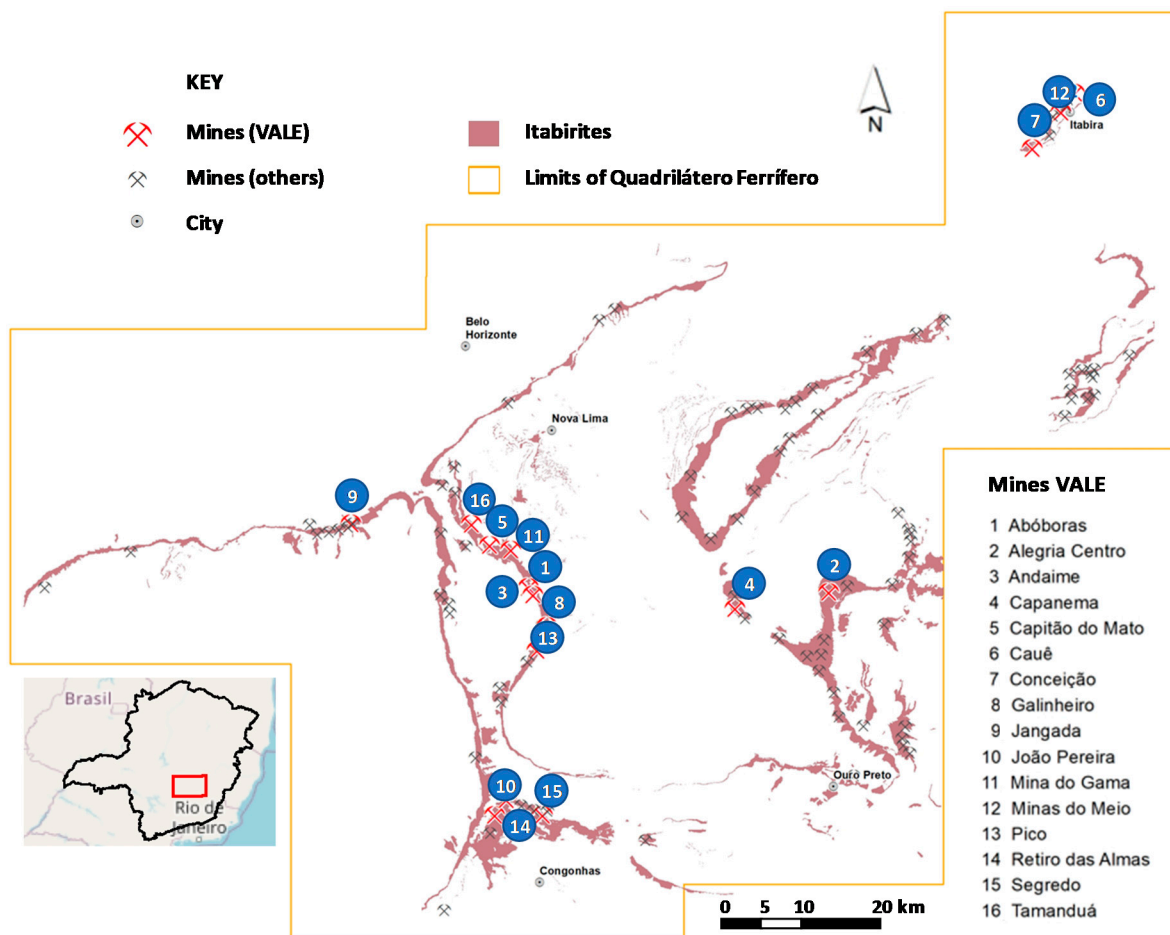


Figure 1. Location of the Vale’s iron ore mines in Quadrilátero Ferrífero.

The study comprised detailed mineralogical and geochemical analyses as well as the determination of physical properties such as density and porosity. The petrographic analyses were supported by norm mineral proportions calculated by Mineral Norm Calculations (MNC) from chemical analyses. The chemical results of all samples were converted into mineral proportion ( $m_m$ ) using the MNC algorithm which was created by Ribeiro [2] and Ribeiro and Carvalho [3] using BASIC language. The first version of the MNC algorithm was based on Voicu [4] methodology to evaluate the mineral assemblage contained in a laterite soil profile from sub-tropical regions in Africa. Motta [5] compared the results of MNC mineral proportions with Optical Microscopic Counting (OMC) methods and obtained good correlations.

The extensive volume of information generated by the Compact Itabirite Project increased the knowledge about the stratigraphy of the unweathered BIFs of the Paleoproterozoic Cauê and Gandarela Formations of the Itabira Group, Minas Supergroup. However, this information is still not in the public domain. Based on the petrographic analyses of

non-weathered itabirite samples, the following sequence of deposition was recognized: dolomite itabirite (IDO), dolomite-quartz itabirite (IC), quartz-dolomite itabirite (IDS), and hematite/magnetite-quartz dolomite (DO) (Vale, internal reports). In addition, it provided the data required to assess the effect of weathering on those rocks, which in turn allowed the revision of the methodology used in geological modeling and resource estimation.

Chemical assays of 717 samples from the project “Geology of Compact Itabirites in the Quadrilátero Ferrífero (QF)” were generated and converted into mineral composition using the MNC algorithm. Only 171 samples (23.8%) yielded carbonate on their normative mineral composition and were classified as non-weathered (compact) itabirites. There were five lithological groups identified amongst the non-weathered samples applied to the normative mineralogy: (1) dolomite itabirite; (2) quartz itabirite; (3) dolomite-quartz itabirite; (4) quartz-dolomite itabirite, and (5) quartz dolomite (Table 1).

**Table 1.** Lithological groups and their mineral proportion (MNC)—weathered (w) and unweathered (u) samples.

Litho	Lithology	Samples	Qz. (%)	Carb. (%)	Goet. (%)	Fe ox. (%)	Others (%)
IDO	Dolomite itabirite (u)	29	4.2	46.2	0	48.8	1.2
IC	Quartz itabirite (u)	7	47.8	3.2	0	46.6	2.4
IDSI	Dolomite-quartz itabirite (u)	87	40.0	14.9	0	43.2	1.9
IDO	Quartz-dolomite itabirite (u)	28	29.1	42.4	0	26.3	2.3
DO	Quartz dolomite (u)	20	14.7	69.8	0	11.0	4.5
IC	Weathered quartz itabirite(w)	546	44.9	0	10.7	42.9	1.5

Qz. = quartz, Carb. = carbonates (mostly dolomite), Goet. = goethite, Fe ox. = iron oxides (mostly hematite).

Most of the geochemical analyses (76.2%) yielded weathered rocks when the MNC algorithm was applied. They correspond to samples of weathered quartz itabirite, with hematite as the main iron mineral, plus quartz and goethite (Table 1). The lack of carbonates and the presence of goethite in this group is evidence of the leaching of minor carbonate and sulphide from the original rock and precipitation of iron hydroxides in the porous matrix during the weathering process. The presence of Mn-rich itabirite in this group (4.8% of weathered samples) is another indication of the carbonate leaching from the protolith, as Mn<sup>4+</sup> has low mobility and is promptly precipitated from weathering solutions during weathering of carbonate-bearing itabirites [6].

The use of the average bulk density of the different rock types was the traditional method applied by Vale’s resource geologists to evaluate the mass of the lithologies in the block model until 2015. The method works well to estimate large volumes of rocks, but it has issues in the local estimation of small volumes when a low number of samples is available, or spatial clustering of samples is present. Motta et al. [7] applied the MNC method combined with grain size partition of mineralogy to calculate the absolute or mineral density, bulk density, and porosity of iron ore samples. These authors have suggested a new low-cost solution to estimate indirectly the mineral density and total porosity of the samples, improving the reconciliation of mass between the geological model and production results. In addition, the number of density samples available to estimate the density in the block model has increased from hundreds (real density samples measured in the field) to thousands (density samples calculated via the MNC algorithm, using the chemical analyses), without additional expense.

After 2016, in order to validate the results obtained by Motta [5] with iron ore samples and expand the use of the algorithm to other weathered rocks, the scope of the “Compact Itabirite Project” has focused on mineral characterization, rock porosity estimation and density quantification, using weathered and non-weathered samples. The aim of

this manuscript is to introduce the methodology applied in the study and to establish correlation rules between the different types of supergene iron ores and their fresh rock equivalents. We report new in situ density, moisture, modal mineralogy, and porosity data of representative weathered and non-weathered itabirite samples, which will contribute to better understanding of the genetic constraints of the major iron ore deposits in QF. This information is critical to (i) improve geological modeling procedures, minimizing the risk in the economic evaluation of iron ore reserves; (ii) assess the porosity and saturation behavior of the different types of itabirite and country rocks and their impacts on the mineral resources estimation. Furthermore, we updated the algorithm for Mineral Norm Calculation (MNC), incorporating the estimation of the modal mineralogy of carbonate-bearing itabirite samples, which was validated by X-ray Powder Diffraction (XRD) with Rietveld refinement and SEM-based automated mineralogy analyses through quantitative evaluation of materials by scanning electron microscopy (QEMSCAN).

## 2. The Genesis of Friable and Supergene Iron Ores

The genesis of friable iron ores has been the subject of debate for many years and is attributed to a combination of hypogene and supergene processes [6,8,9]. Although hypogene models have been proposed by some authors [10–12], the supergene model is regarded as a reference to the origin of friable ores such as “hematite”, quartz itabirite, goethite itabirite, and manganeseiferous itabirite [8].

Guild [13] postulated that the dissolution of carbonates from carbonate-bearing itabirite and country rocks by meteoric waters provides alkaline conditions to dissolve quartz of unweathered itabirites to generate friable itabirites. Dorr and Barbosa [11] suggested that friable iron ores derive from originally unweathered high-grade ores (called “hard hematite”) by supergene leaching “of small quantities of hematite at crystal boundaries, thus disaggregating the rock”. A suggestion that friable itabirites result from leaching of unweathered itabirites with different carbonate content, grain size, and varied proportion of hematite and quartz, was presented by Pomerene [14]. The alteration or supergene leaching of initially hard, but porous high-grade “hematite”, was postulated by Dorr [15] as the origin of soft ores (soft ore is another term commonly used in the QF to designate friable ores).

Barbour [16] observed that the oxidation of magnetite produces martite and that the overall weathering degree of itabirite decreases with depth, due to secondary surface processes. According to Varajão et al. [17,18] and Morris [19,20], the martitization of magnetite occurs under supergene conditions. Ribeiro [2] proposed a supergene Fe-enrichment of the itabirite, by quartz and carbonate leaching, through a dissolution process. This leaching process would be accompanied by the formation of slump structures, such as kink-bands, and would generate small to medium size karst depressions. The depressions would then be filled by detrital clays and gravels of compact iron ore and itabirite. Cenozoic sedimentary basins formed by karst processes and covering itabirite and iron ore are spread in the QF [21–23] and references within. Some of them are mined for bauxite.

Viel et al. [24] highlighted the significance of preferential dolomite leaching and structural controls on the genesis of soft iron ores. Ribeiro and Carvalho [3] noted that the steep dip of the itabirites favors the infiltration of meteoric water and the dissolution of carbonates, amphiboles, and quartz from the rock, decreasing the cohesion between grains and bands. As the weathering process progresses, the hematite-rich laminae and residual quartz become isolated, and the itabiritic rock collapses [3]. The subsidence of the system is therefore governed by volume losses, and the volume collapsed can be calculated. This calculation takes into account the original volume of each mineral and void in the fresh rock and the final mineral volume, free water, and voids in the altered rock.

Ribeiro and Carvalho [3] developed a numerical leaching model to simulate the volume loss of itabirite during the weathering process, using a compact vertical 2D banded matrix, composed of 50% on volume of leachable nodes (carbonate, amphiboles, and quartz) and 50% of non-leachable nodes (hematite).

Spier et al. [25] applied  $^{40}\text{Ar}/^{39}\text{Ar}$  geochronology to date Mn-oxides formed during weathering of itabirite and dolomites of the Cauê and Gandarela Formation. The authors noted that weathering profiles overlying iron ore deposits in the QF reach depths of 150–400 m and have been developed since at least 62 Ma, with a major development period between 51 and 41 Ma.

### 3. Methodology

#### 3.1. Sample Selection and Analytical Procedures

After the year 2015, a total of 366 drill hole and channel samples of itabirite and iron ore were selected from 13 iron ore deposits owned by Vale in the QF (Figure 1). The 366 samples were divided into 3 subgroups: the first subgroup contained 167 samples of weathered iron ore/itabirites, all of them friable materials. They were collected on the surface of active open-pit mines and comprised friable hematitite (HF), friable quartz itabirite (IF), friable Fe-rich quartz itabirite (IFR), goethite-bearing itabirite (IGO), Al-rich itabirite (IAL), and Mn-rich itabirite (IMN). The second subgroup included 139 drilling samples of compact rocks (weathered), composed of compact hematitite (HC) and quartz itabirite (IC). Finally, the third subgroup contained 60 samples of compact carbonate types (unweathered), comprised of quartz dolomite (DO), dolomite itabirite (IDO), quartz-dolomite itabirite (IDR), dolomite-quartz itabirite (IDS), and dolomite hematitite (HDO). From this universe (of all 366 samples), 83 samples were selected for direct mineral quantification by X-ray diffraction (XRD) and SEM-based automated mineralogy (QEMSCAN): 28 carbonate types (dolomites or itabirites) and 55 iron oxide types (compact and friable hematitites and itabirites). This selection honors the diversity of chemical and mineral composition of the total sample database.

Chemical assays for the 366 samples were obtained in the laboratories of Vale on duplicate samples, via X-ray fluorescence on pressed pellets, and the loss on ignition was determined following gravimetric procedures.

#### 3.2. Mineralogy Calculations Using the MNC Algorithm

The conversion of chemical analyses into mineral composition has long been used and is described in the literature [4,5,7]. The assumptions applied in our MNC algorithm considered two possibilities: weathered rocks lacking carbonate minerals and unweathered, carbonate-bearing rocks. The algorithm, which was developed internally in BASIC programing language, was applied to each sample considering the two alternatives. The samples were classified as weathered or non-weathered, based on the presence of carbonate in the calculated mineralogy (Figure 2). For this purpose, it was assumed that carbonate-bearing rocks are non-weathered and that all other rocks were weathered. We use the term “oxide” interchangeably with weathered to designate this second group. It may include samples of partially weathered quartz itabirite, called compact or semi-compact quartz itabirite.

A simplified version of the MNC algorithm for weathered samples contemplates in the calculations below and in the Appendix A Figure A1:

- i. Magnetite content from FeO grade—Residual Fe\_i;
- ii. Kaolinite content from LOI,  $\text{Al}_2\text{O}_3$  and  $\text{SiO}_2$  grades—Residuals  $\text{SiO}_2\text{-i}$ ,  $\text{Al}_2\text{O}_3\text{-i}$  and  $\text{LOI-i}$ ;
- iii. Gibbsite content from  $\text{LOI-i}$  and  $\text{Al}_2\text{O}_3\text{-i}$  grades—Residuals  $\text{LOI-ii}$ ;
- iv. Quartz content from  $\text{SiO}_2\text{-i}$ ;
- v. Pyrolusite content from Mn grade;
- vi. Goethite content from Fe\_i and  $\text{LOI-ii}$ —Residual Fe\_ii;
- vii. Hematite content from Fe\_ii residual grade



**Figure 2.** Illustration of how the chemical composition of the samples was allocated to the different minerals for weathered (left column) and unweathered (right column) materials. The density assumed for each mineral in the Mineral Norm algorithm (MNC) is shown on the right of the figure.  $V_{Mi}$  = mineral volume,  $M_{Mi}$  = mineral mass,  $\rho_{Mi}$  = mineral density.

The MNC applied to carbonate rocks assumes:

- i. Clinochlore content from  $Al_2O_3$  grade—Residuals  $FeO_{-i}$ ,  $Fe_{-i}$ ,  $SiO_2_{-i}$ ,  $MgO_{-i}$  and  $LOI_{-i}$ ;
- ii. Ankerite from Mn grade—residuals— $FeO_{-ii}$ ,  $LOI_{-ii}$ ,  $CaO_{-i}$ ,  $MgO_{-i}$ ;
- iii. Magnetite from  $FeO_{-i}$  grade—residuals  $Fe_{-ii}$ ;
- iv. Dolomite from  $CaO_{-i}$  grade—residuals  $LOI_{-iii}$  and  $MgO_{-ii}$
- v. if  $MgO_{-ii} < 0$  than Dolomite from  $MgO_{-ii}$  grade—residual  $CaO_{-ii}$  and  $LOI_{-iii}$ ;
- vi. Calcite from  $CaO_{-ii}$  grade—residual  $LOI_{-iv}$ ;
- vii. if step v is true Talc from  $MgO_{-ii}$  grade—residuals of  $SiO_2_{-ii}$
- viii. Quartz content from  $SiO_2_{-i}$  or  $SiO_2_{-ii}$ ;
- ix. Pyrolusite content from Mn grade (optional instead of ankerite);
- x. Hematite content from  $Fe_{-ii}$  residual grade

### 3.3. Bulk and Mineral Densities and Total Porosity Measurements

Two methods were applied to measure the in situ density of the samples: filling volume (FV) for friable materials, and hydrostatic balance (HB) for compact samples [26,27]. These tests have, in general, different supports: the HB method uses a cylindrical specimen from diamond drilling cores (approximately 20 cm long and 7 cm wide), whereas the FV method uses an excavated pit and generates a cubic sample with approximately 20 cm edge. Both methods require homogeneity and regular shapes in order to reduce the bias of volume measurements.

The ratio between sample mass ( $m$ ) and volume ( $v$ ) is considered as the natural or in situ density on a wet basis ( $\rho_n$ ), and the ratio between the dried mass ( $m_s$ ) and volume is the in situ density on a dry basis ( $\rho_s$ ) (Equations (1) and (2)). The moisture ( $u$ ) is given by the proportion of free water compared to the total mass (Equation (3)).

$$\rho_n = \frac{m}{v} \quad (1)$$

$$\rho_s = \frac{m_s}{v} \quad (2)$$

$$u = \frac{m - m_s}{m} \quad (3)$$

The total porosity ( $\phi$ ) of the sample can be indirectly accessed by the relation between the in situ dry bulk density ( $\rho_s$ ) and the mineral or absolute density ( $\rho$ ) as shown in Equation (4). The free water porous saturation ( $\phi_s$ ) is calculated by the proportion of the volume of water in relation to the total porosity (Equation (5)).

$$\phi = 1 - \left( \frac{\rho_s}{\rho} \right) \quad (4)$$

$$\phi_s = \frac{\rho_n - \rho}{\phi} \quad (5)$$

Two methods were used to estimate the mineral density ( $\rho$ ): gas pycnometer and through specific weight ( $\rho_m$ ) of each mineral and its respective mass proportion calculated by MNC or Rietveld (XRD). Pycnometry was carried out at an internal Vale laboratory according to ASTM D5550-14 norm, using Helium gas. The samples were ground to  $-0.045$  mm, dried in a furnace at  $105^\circ\text{C} \pm 5^\circ\text{C}$ , and analyzed in a cylindrical volume with  $60\text{ cm}^3$ . The mineral density of the samples was obtained by the sum of the mineral proportion ( $m_m$ ) divided by the sum of the mineral volumes ( $v_m$ , Equation (6)), which was calculated by mineral proportion divided by the specific weight of each mineral ( $\rho$ , Equation (7)).

$$\rho = \frac{\sum_{i=1}^n (m_{m_i})}{\sum_{i=1}^n (v_{m_i})} \quad (6)$$

$$v_m = \frac{m_m}{\rho_m} \quad (7)$$

where,  $i$  = mineral index and  $n$  = number of minerals.

#### 4. Results

##### 4.1. Validation of Mineral Density, Porosity, and Porous Saturation by Comparison of MNC Versus Pycnometry (PYC) Measurements

To validate the MNC methodology to estimate mineral density, pore saturation and porosity, the chemical, bulk density and moisture database of 306 samples was used. Such data were collected after the year 2016. The average mineral density and porosity for weathered 306 samples (167 friable and 139 compact material) are shown in Table 2.

**Table 2.** Average mineral density ( $\rho$ ) and porosity ( $\phi$ ) by lithology and measurement method—weathered samples—subgroups 1 (friable) and 2 (compact).

Lithology	Samples	$\rho$ MNC (g/cm <sup>3</sup> )	$\rho$ PYC (g/cm <sup>3</sup> )	$\phi$ MNC (%)	$\phi$ PYC (%)
Compact hematite	37	4.92	4.95	6.89	7.45
Friable hematite	20	4.96	5.03	37.32	38.17
Al-rich itabirite	5	4.14	4.27	36.27	38.22
Quartz itabirite	102	3.63	3.65	6.98	7.38
Friable quartz itabirite	96	3.90	3.93	32.38	32.99
Fe-rich friable quartz itabirite	28	4.45	4.47	38.98	39.31
Goethite itabirite	4	3.80	3.85	43.98	44.73
Mn-rich itabirite	14	3.96	4.03	34.73	35.71
Total	306	4.06	4.09	22.08	22.64

MNC = mineral normative calculation, PYC = pycnometry.

To analyze the free water saturation of porous only the group composed of 167 friable samples were used and the results are shown in Table 3. For the unweathered group (60 carbonate samples), the averages are shown in Table 4. The averages were calculated per lithology, using two methods: MNC and PYC. The Appendix A Table A1 shows a complete dataset for weathered samples and Appendix A Table A2, unweathered samples of the deposits.

**Table 3.** Average pore saturation ( $\phi_s$ ) and moisture ( $u$ ) by lithology and measurement method—weathered samples—subgroup 1 (friable).

Lithology	Samples	$\phi_s$ MNC (%)	$\phi_s$ PYC (%)	$u$ (%)
Friable hematite	20	60.21	58.88	7.00
Al-rich itabirite	5	84.94	79.47	10.17
Friable quartz itabirite	96	36.43	35.45	4.40
Fe-rich friable quartz itabirite	28	52.75	51.45	7.07
Goethite itabirite	4	67.53	66.37	12.65
Mn-rich itabirite	14	56.43	54.87	7.33
Total	167	45.89	44.63	5.78

**Table 4.** Average mineral density ( $\rho$ ) and porosity ( $\phi$ ) by lithology and measurement method—subgroup 3—unweathered (carbonate) samples.

Lithology	Samples	$\rho$ MNC (g/cm <sup>3</sup> )	$\rho$ PYC (g/cm <sup>3</sup> )	$\phi$ MNC (%)	$\phi$ PYC (%)
Quartz dolomite	11	2.98	3.00	5.40	6.30
Dolomite hematite	13	4.87	4.76	7.34	5.38
Dolomite itabirite	7	3.69	3.70	4.06	4.53
Quartz-dolomite itabirite	17	4.42	4.34	6.36	4.72
Dolomite-quartz itabirite	12	3.50	3.49	5.71	5.47
Total	60	3.98	3.94	6.00	5.28

Excellent correlations between MNC and PYC methods were observed for these three parameters, mineral density, porosity, and pore saturation, as seen in the scatter diagrams in Figure 3a–c, respectively. The diagram in Figure 3d correlates moisture and saturation using PYC data, displaying a nonlinear correlation and high dispersion of the points around the equation line. This behavior is caused by the climate effect during the sampling. Figure 3a,b correspond to the friable and compact altered samples from Table 2 and Figure 3c,d consider the friable samples from the Table 3. The correlations between PYC and MNC methods for carbonate samples (Table 4) are excellent for density values and acceptable for porosity (Figure 4left,right, respectively).

#### 4.2. Mineralogical Composition via XRD/Rietveld and QEMSCAN

For the mineralogical analysis, 83 samples were separated into two groups of itabirites: unweathered (carbonate) and weathered. The carbonate group is formed by 28 samples from 3 mines, comprising dolomite itabirite (IDO), quartz-dolomite itabirite (IDR), dolomite hematite (HDO), and dolomite (DO). The weathered group is composed by 57 samples from 7 mines, and comprised of compact quartz itabirite (IC), friable quartz itabirite (IF, IFR), compact hematite (HC), and contaminated itabirites: goethitic (IGO), manganiferous (IMN), and aluminous (IAL). The correlations between mineral proportion calculated for both groups by MNC and XRD are shown in Figures 5 and 6.

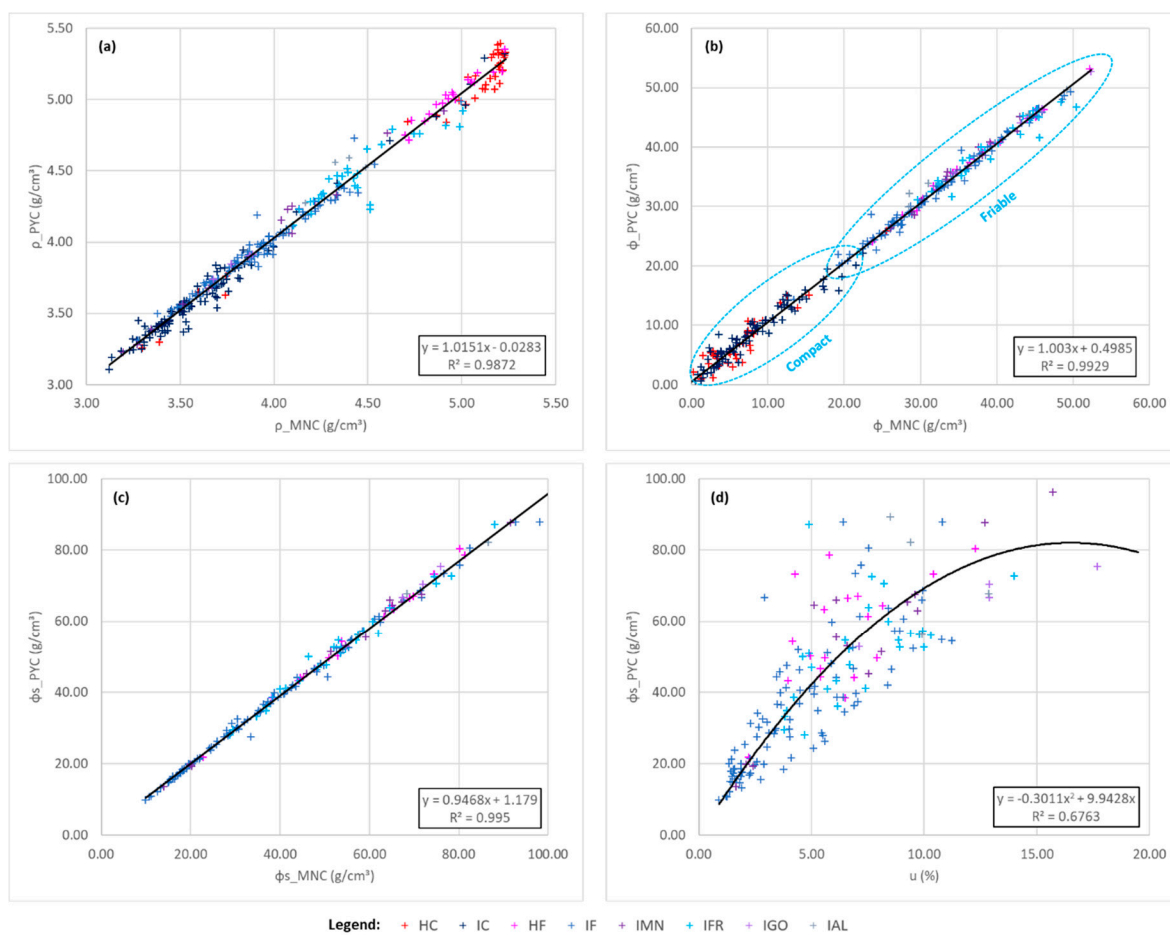


**Figure 3.** Scatter diagrams mineral density (a), porosity (b)—data from the Table 2 (subgroups 1 and 2), and saturation (c) calculated by MNC (Mineral Norm Calculations) and PYC (Pycnometry) methods, and moisture and saturation of PYC method (d)—data from the Table 3 (subgroup 2).

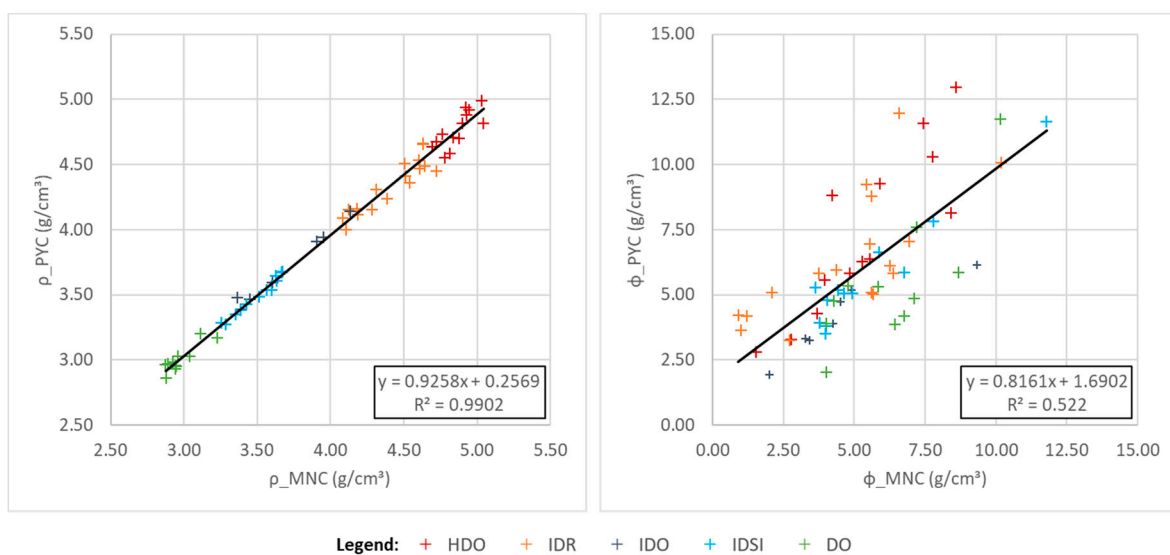


**Figure 4.** Scatter diagrams of mineral density (left) and porosity (right) calculated by MNC and PYC methods, using carbonate samples—data from the Table 4—(subgroup 3).

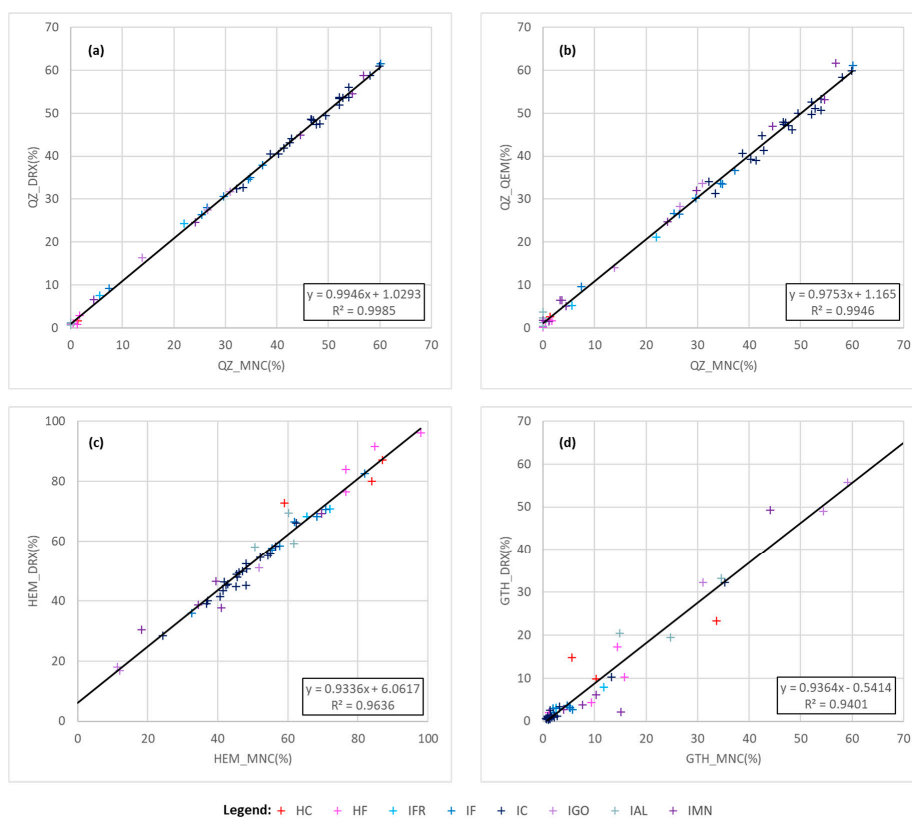


**Figure 5.** Scatter diagrams mineral proportions of quartz (**a,b**), hematite (**c**) and goethite (**d**) calculated by MNC-weathered and XRD/Rietveld (left side) or QEMSCAN (right side) methods using weathered samples.

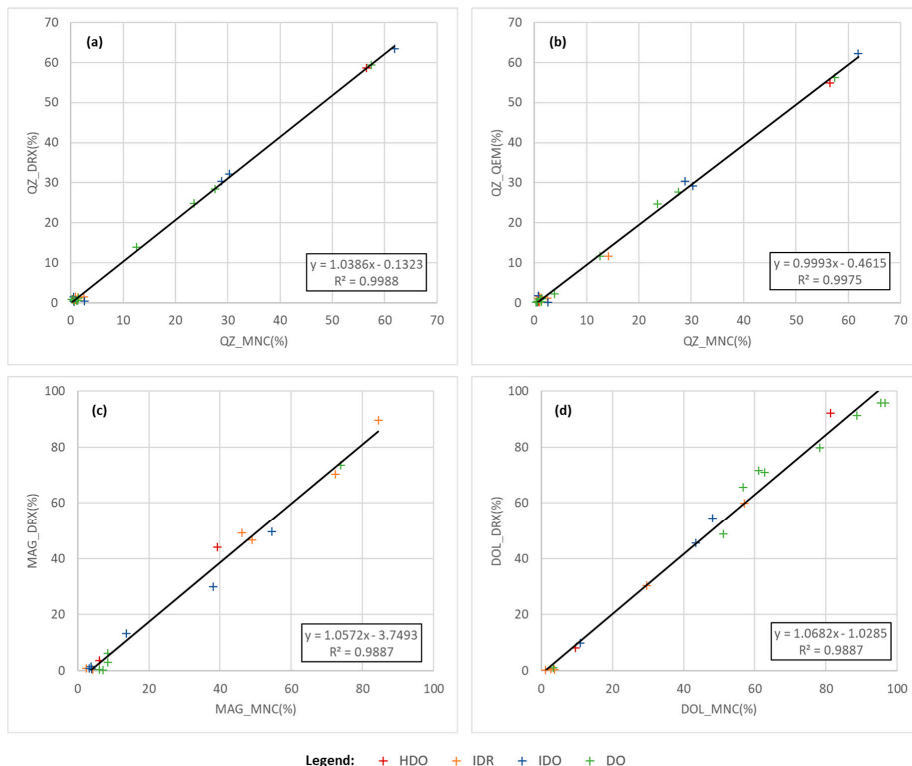


**Figure 6.** Scatter diagrams comparing mineral proportions of quartz (**a,b**), magnetite (**c**), and dolomite (**d**), calculated by MNC and XRD/Rietveld or QEMSCAN methods using unweathered (carbonate) samples.

The correlation between the normative results (MNC) and the mineral proportions obtained via XRD for the main minerals (quartz, hematite, magnetite, dolomite, and goethite) is very high. There is a very low global bias (similar averages) and conditional bias (similar standard deviations), for both unweathered (carbonate) and weathered groups. Figures 7 and 8 show the mineral proportions obtained via XRD/Rietveld method for weathered and unweathered (carbonate) groups, respectively. Manganous itabirite is an industrial classification for friable ore with Mn grade higher than 1% and the calcite hematite/magnetite samples can be associated with the dolomite hematite hydrothermal ore group.

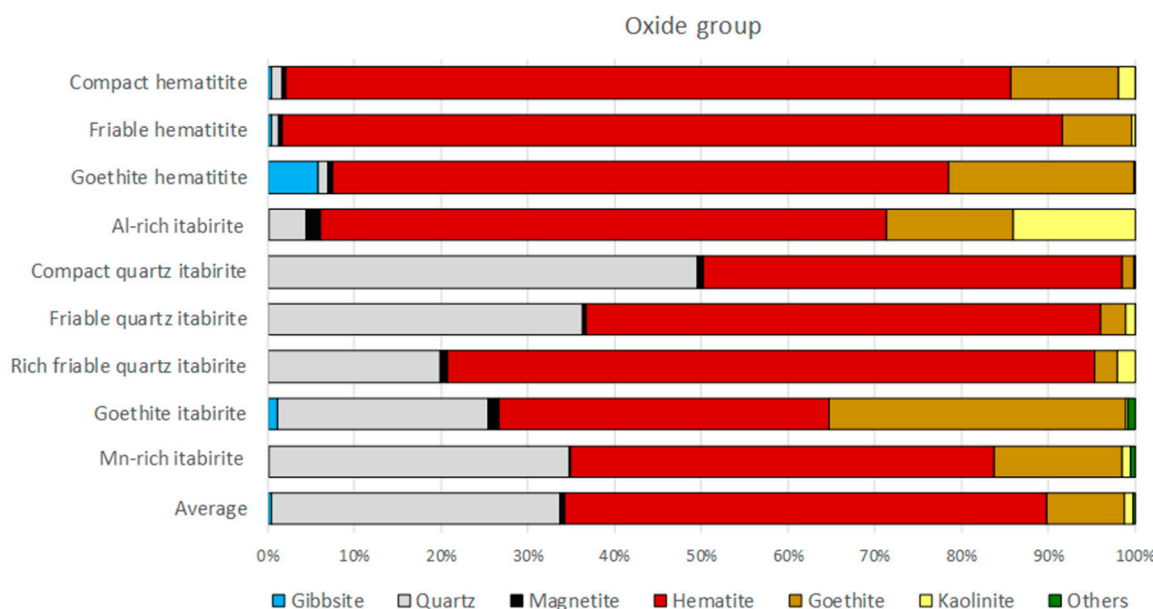


**Figure 7.** Average mineral proportions (wt. %) by XRD/Rietveld—weathered materials.

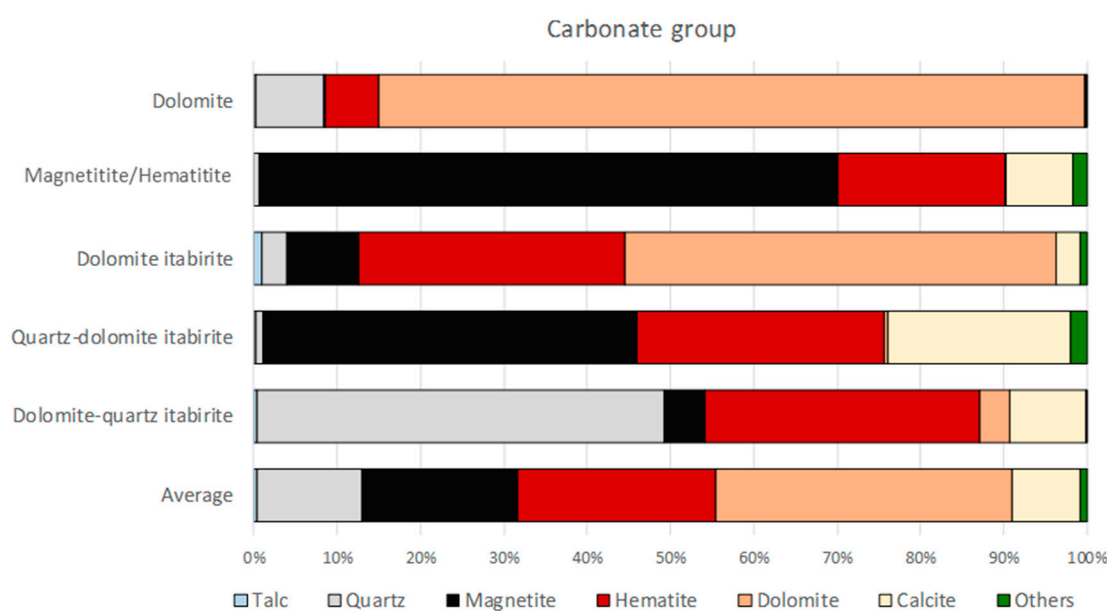


**Figure 8.** Average mineral proportions (wt. %) by XRD/Rietveld—unweathered (carbonate) materials.

For the weathered group, the mineral assembly obtained via XRD contains hematite, quartz, and goethite as the main components, in different proportions. The siliceous

lithotypes (compact quartz itabirite, friable quartz itabirite, and rich, friable quartz itabirite) have quartz as the main non-ferrous mineral and low content of magnetite (less than 2% on average). The compact siliceous lithotype has on average 50% quartz, and there are no significant iron hydroxides and manganese oxides in its composition. In the contaminated itabirites (Mn-rich itabirite, Al-rich itabirite, and goethite itabirite) and hematite-bearing lithotypes (high-grade ores, >62 wt. % Fe) (compact hematitite, friable hematitite, and goethite hematitite), the proportions of manganese oxides, gibbsite, kaolinite, and iron hydroxides increase significantly.

The unweathered itabirite group (dolomite itabirite, dolomite hematitite, quartz-dolomite itabirite, and dolomite-quartz itabirite) has magnetite and/or hematite and carbonates (dolomite, calcite, and ankerite) in different proportions. The rich types (quartz-dolomite itabirite and dolomite hematitite) have a high content of magnetite (45% and 69%, respectively). All samples are compact and display no significant weathering features.

#### 4.3. The Correlation between Weathered Iron Ores and Their Likely Protoliths via Simulation of the Weathering Process

The quantitative effects of weathering in itabirites can be assessed considering the mineral composition and porosity in correspondent volumes of weathered and fresh rocks. The algorithm to perform the link between fresh itabirites/dolomites and weathered rocks [2,5,7] is based on the measurements of similarities between iron ore samples (actual samples) and the simulated product of weathering from different types of fresh itabirites and dolomites. Assuming that the moisture represents free water inside voids in a given volume proportion, it is possible to estimate the final mass proportion of the weathered material resulting from leaching of carbonates from the original quartz dolomite. The algorithm contemplates the following steps on its execution:

- (1) Mineral norm calculation from chemical assays of fresh rocks of a given iron deposit
- (2) Estimation of mass proportions of minerals and the final real density of rock
- (3) Estimation of volume proportions of minerals
- (4) Leaching of mobile chemical components in the weathering zone (CaO, MgO and LOI)
- (5) Residual re-estimation of low mobile elements in the weathering zone (Al, Fe, Si, Mn, P)
- (6) For each specific weathered sample group, the most similar pair of fresh samples, considering the low mobile elements grades re-calculated in (5)
- (7) Porosity of weathered sample—Evaluation from the MNC equation obtained in the experimental data
- (8) Collapse volume (C)—Evaluation based on the total volume of stable minerals ( $v_1$ ), porosity ( $\phi_1$ ), and volume of carbonates ( $vc_1$ ) from fresh rock and volume of minerals ( $v_2$ ) and porosity ( $\phi_2$ ) from the equivalent pair of the weathered ore, according to the following equation:

$$C = vc_1 + \phi_1 - \left( \phi_2 \cdot \frac{v_1}{v_2} \right) \quad (8)$$

- (9) Analysis of the spatial distribution of samples and link between weathered and fresh protoliths.

An example illustrating the application of the algorithm is shown in Figure 9. This figure shows, in six steps, the sequence to transform original quartz dolomite (fresh sample pair with  $v_1 = 22\%$ ,  $\phi_1 = 6\%$ , and  $vc_1 = 72\%$ , Figure 9a,b) into friable quartz itabirite (weathered pair with 36% of residual total porosity,  $\phi_2$ , and  $v_2 = 64\%$ , Figure 9d), 8% of moisture (Figure 9f), and approximately 65% of volume collapse (Figure 9c).

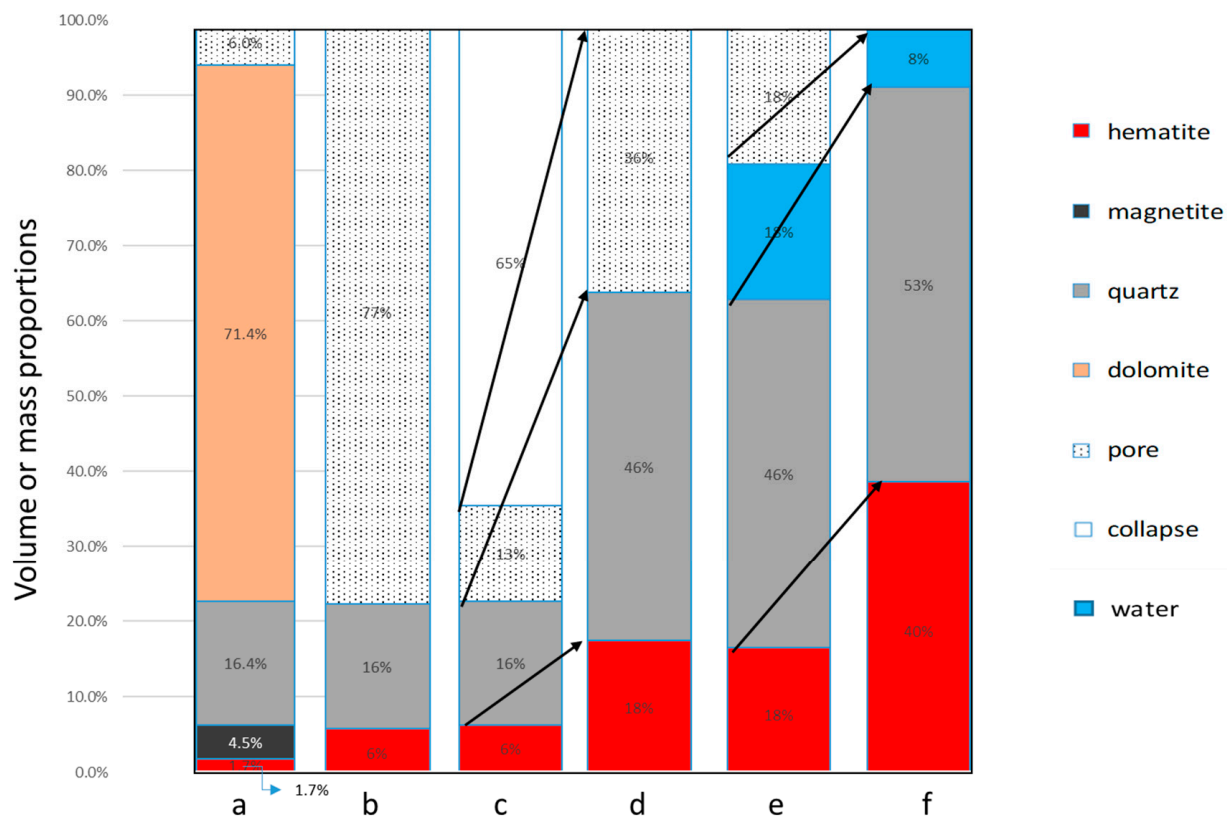


**Figure 9.** **a** volume proportion of non-weathered quartz dolomite; **b** hypothetical void generation after dolomite leaching if collapse is unconsidered; **c** collapse volume and actual void volume in residual rock volume proportion; **d** residual volumes of mineral and voids (porous) in weathered rock; **e** volumes of mineral, wet and dry voids (porous) in weathered rock; **f** residual mass proportion of minerals and water in weathered rock.

Considering a typical supergene hematite ore with total porosity ( $\phi_2$ ) equal to 35.6% and the sum of volumes of hematite (54.2%) and quartz (10.2%) equal to 64.4% ( $v_2$ ) and a dolomite itabirite composed of 6% of porosity ( $\phi_1$ ), and volumes of carbonate, iron oxide, and quartz equal to 56.4%, 32.1%, and 5.5%, respectively ( $v_1 = 37.6\%$ ), the collapse volume calculated by the equation 10 is 41% from the original volume of the fresh rock, as shown in Figure 10. These calculations suggest that friable hematite is formed mainly by leaching of carbonate from the dolomite itabirite, supporting the conclusions made by Spier et al. [6,8] regarding the genesis of this rock. They also suggest that dolomite quartz-itabirite originates from the compact quartz itabirite with medium porosity or the friable quartz itabirite with high porosity, depending on the amount of quartz on the original protolith (Figure 11). The origin of Fe-rich friable quartz itabirite can be linked to quartz-dolomite itabirite with low content of quartz (Figure 12). Mn-rich and goethite itabirites are associated too with the leaching of dolomites and quartz dolomites whose carbonates have iron and manganese in their composition (Fe-dolomite and ankerite). Table 5 shows the correlation between samples of weathered lithological groups with their likely protoliths and respective calculated collapses, considering a null porosity of the protoliths ( $\phi_1 = 0$ ) by simplification.

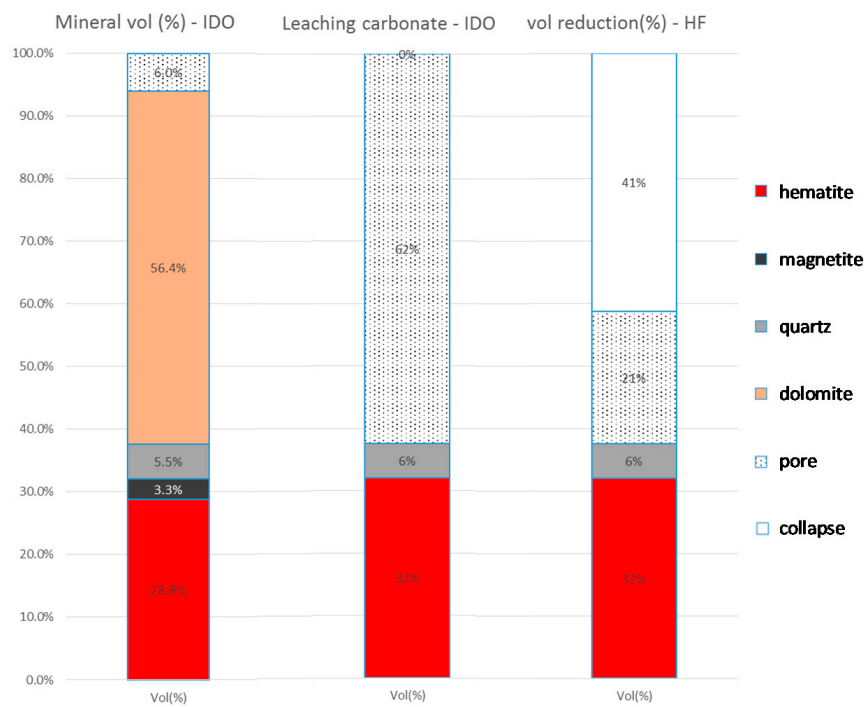


**Figure 10.** Original mineralogy and porosity in a volume of dolomite itabirite (IDO), leaching volume and friable product hematite (HF) with 36% of porosity and 41% of original volume collapsed.

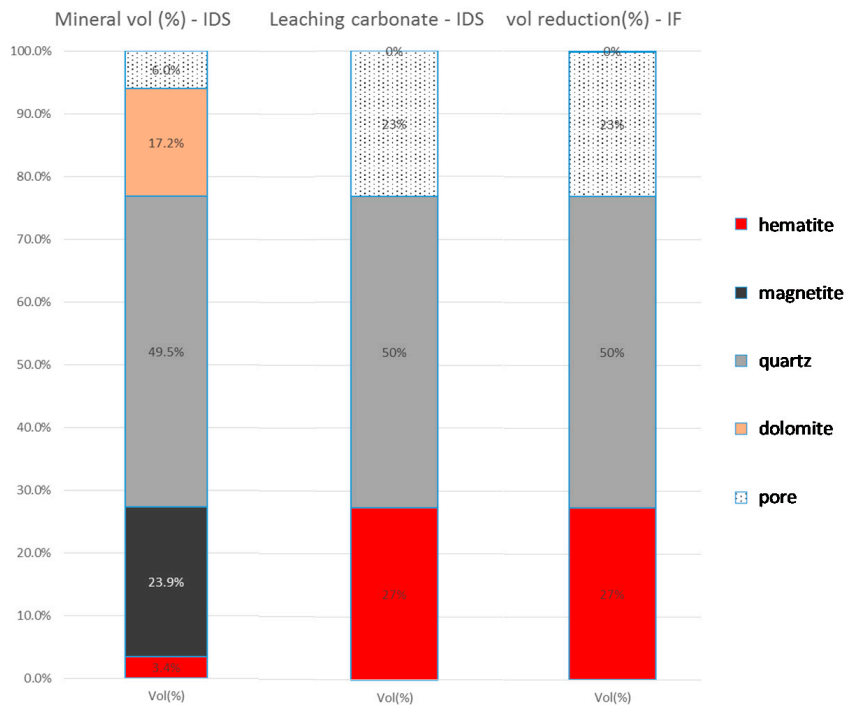


**Figure 11.** Original mineralogy and porosity in a volume of quartz-dolomite itabirite (IDS), leaching volume, and final result friable quartz itabirite (IF) with 23% of porosity without significant collapse.

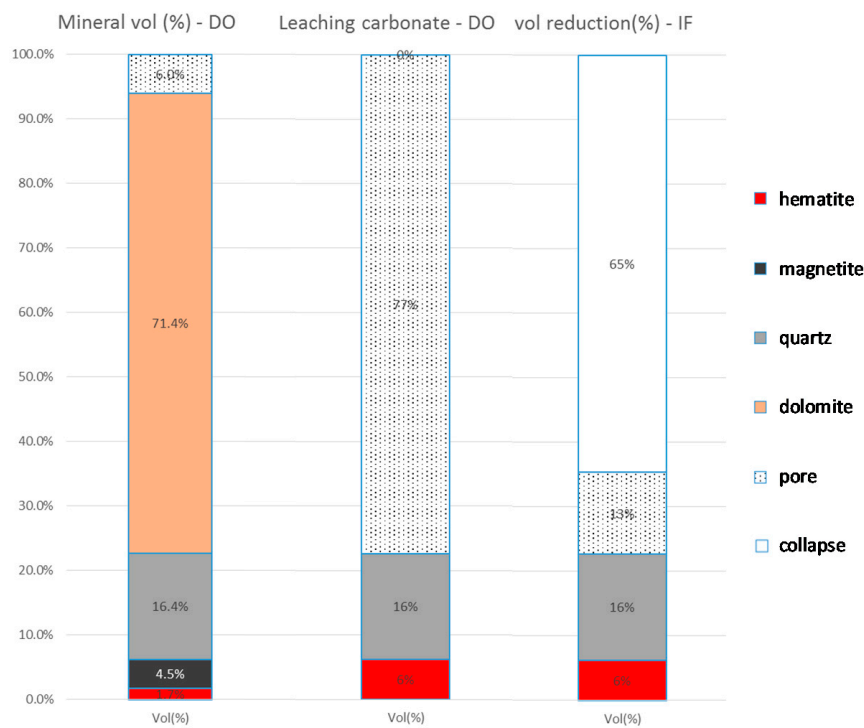


**Figure 12.** Original mineralogy and porosity in a volume of dolomite (DO), leaching volume, and final result friable quartz itabirite (IF) with 36% of porosity and 65% of original volume collapsed.

**Table 5.** Average calculated mineralogical composition (only main components) and porosity of the studied materials, estimated collapse, and their likely protolith with null porosity ( $\phi_1 = 0$ ).

Weathered Material	Samples	Average Composition of Main Minerals and Pores			Estimated Collapse (Vol. %)	Likely Protolith		
		Calc. Minerals (Vol. %)						
		Fe ox. (v1%)	Qz. (v1%)	Carb. (vc1%)				
Compact hematite	37	82.1	9.9	8.1	6.8	Dolomite hematite		
Friable hematite	20	37.7	1.1	61.2	34.4	Dolomite itabirite		
Friable quartz Itabirite	96	25.0	25.4	49.6	30.3	Quartz-dolomite itabirite		
Semi-compact Quartz itabirite	102	35.7	56.4	8.0	7.0	Quartz itabirite		
Fe-rich friable Quartz itabirite	51	27.16	10.20	62.65	35.19	Qz dolomite		

Fe ox. = iron oxides (mostly hematite), Qz. = quartz, Carb. = carbonates (mostly dolomite).

The tetrahedron in Figure 13 shows the relative volume contents of magnetite, hematite, carbonates, and quartz in fresh materials and their respective weathered products. The points in the graph are the centroids of the cluster groups from 717 samples. The figure also shows an interpretation of Vale's geologists of a potential sequence of deposition of the original BIFs and associated carbonate rocks in the QF.

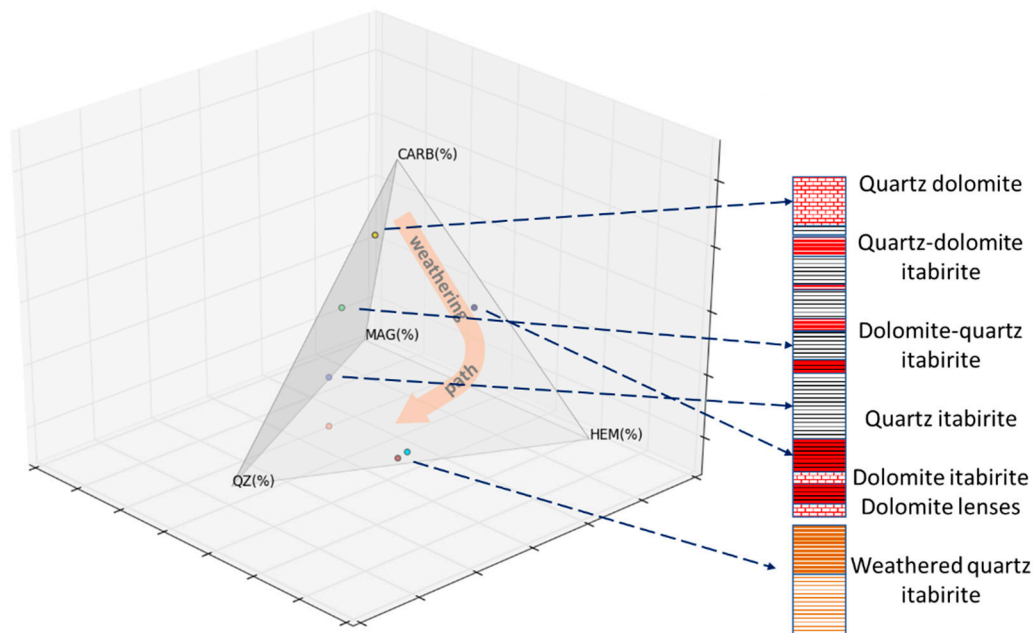


**Figure 13.** Tetrahedron of relative proportions of hematite, carbonates, magnetite and quartz (vol. %) showing fresh and weathered lithotypes and their position in the proposed depositional sequence. Each vertex represents 100% of the mineral variable indicated there. A given point inside the tetrahedron has components that are proportional to how close the point is to the corresponding vertex.

Among other factors, such as climate, topography and time, the final fabric and texture of a weathered product are intimately related to its protolith composition. This association represents an important tool for geological modeling and can be used to improve the knowledge of the stratigraphic sequence on the weathered zone of itabirites. Ribeiro [2] and Braga [28] have shown evidence of the development of weathered-related structures and the generation of porosity on itabirites during weathering (Figures 14 and 15). Figure 15a,b, shows the low porosity in a compact quartz itabirite whose origin is associated with the carbonate bands and veins. Figure 15c,d shows a weathered itabirite with high porosity and deformed matrix composed by hematite and quartz bands that are not weathered.

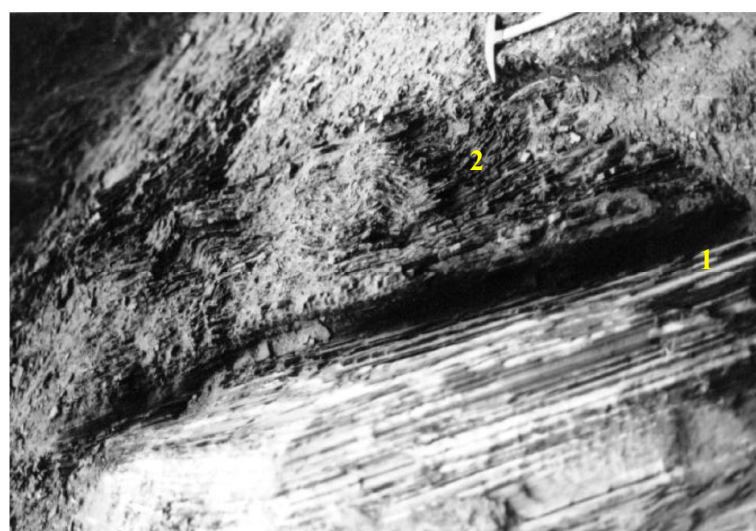


**Figure 14.** Contact between non-weathered/undeformed (1) and weathered/deformed (2) BIF—Pico Mine [2].

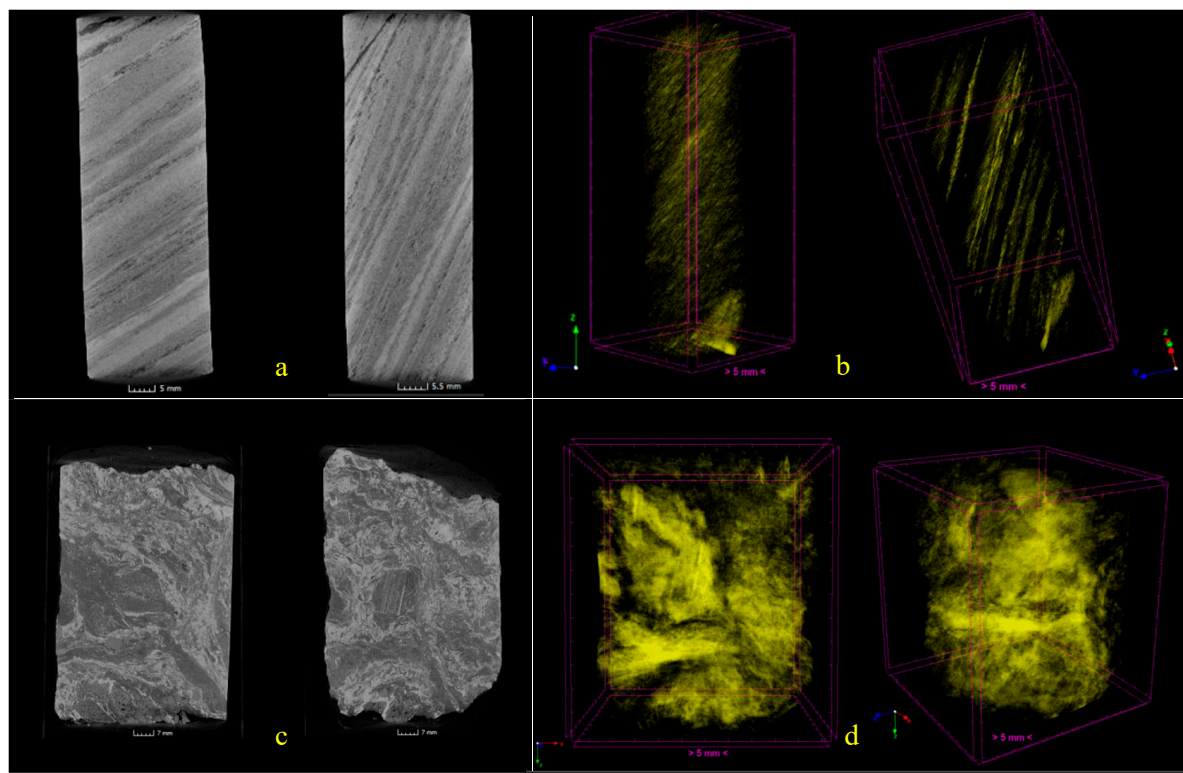


**Figure 15.** Micro-tomography: 2D slice images (**a,c**) and 3D porosity distribution (**b,d**) of partially weathered quartz itabirite (**a,b**) and weathered itabirite (**c,d**)—Abóboras Mine [28].

Scanning electron microscope (SEM) images of the two partially weathered quartz itabirites shown in Figure 15 are presented in Figure 16. The images show the preservation of hematite and quartz from weathering and the formation of highly porous rock. These pores were originally occupied by carbonate [28].

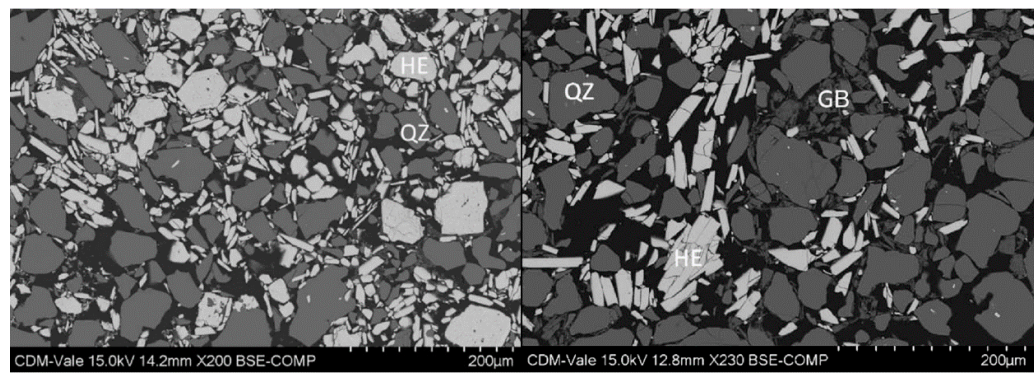


**Figure 16.** SEM images of two weathered itabirites from Abóboras Mine. HE = hematite, QZ = quartz, GB = gibbsite [28].

## 5. Discussion—From Fresh Rock to Weathered Ore

The dissolution of carbonates from the quartz dolomite itabirite by weathering solution is illustrated in Figure 17. There are two steps of weathering in a vertically banded empirical model shown. In contrast to the leaching model algorithm, defined by Ribeiro & Carvalho [3], where leachable vs. non-leachable materials were used, this new model uses three types of materials: two non-leachable (quartz and hematite) and one leachable (carbonate). The amount of leachable and non-leachable minerals is varied in different

zones of the model, with some areas more abundant in carbonate and others in quartz (Figure 17).

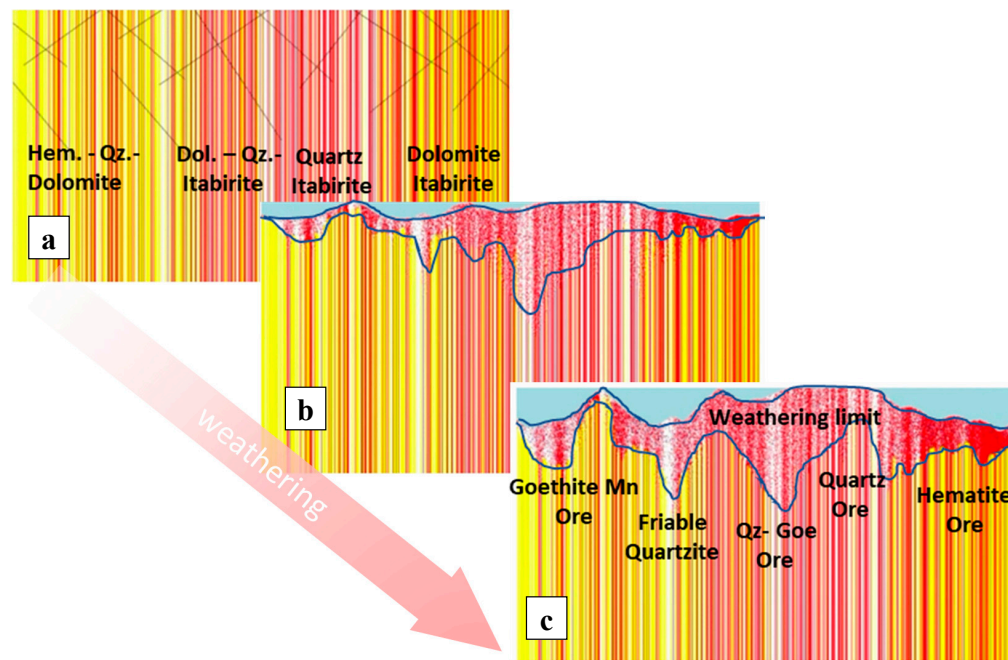


**Figure 17.** Leaching simulation in a 2D original vertical banded matrix, with hematite in red, quartz in white and carbonate in yellow (a). Intermediate leaching of carbonate (b) and final leaching step (c), with the blue area highlighting the collapsed surface.

The model is based on the assumption that the leaching of the carbonate bands leads to a residual concentration of quartz and hematite, as shown in Figures 15 and 16, and that the whole weathered rocks would incrementally collapse, due to gravity. The collapsed material would have a higher amount of hematite and quartz than the original weathered volume. Note the difference between the original topographic surface (flat) with the topographic surface in the advanced weathered stage (hilly) (Figure 17c) and the formation of topographic highs in areas with a greater amount of quartz and hematite in the protolith.

Several simulations using different proportions of leachable and non-leachable minerals suggest that high Fe-grade hematite ores have dolomite itabirite as their protolith. As shown in Figure 18, this rock is frequently found at the base of Cauê Formation. As discussed in Section 4.3, the compact quartz itabirite is likely derived from the weathering of fresh quartz itabirite whose original composition has minor carbonate contribution. The contact between Cauê and Gandarela Formations is transitional [11]. Vale's deep drilling program has identified the occurrence of interfingering lenses of dolomite-quartz itabirite, quartz dolomite, and hematite quartz dolomite in the transitional zone between those stratigraphic units (Vale, internal reports). Our study indicates that the weathering of those rocks would produce porous friable goethite itabirite, Mn-rich itabirites, and friable Fe-rich quartzite, respectively. The geomorphological evolution is controlled by the composition of the protolith. Topographic depressions are associated with carbonate zones, and quartz-rich itabirite controls the formation of topographic high and elevated plateaus.

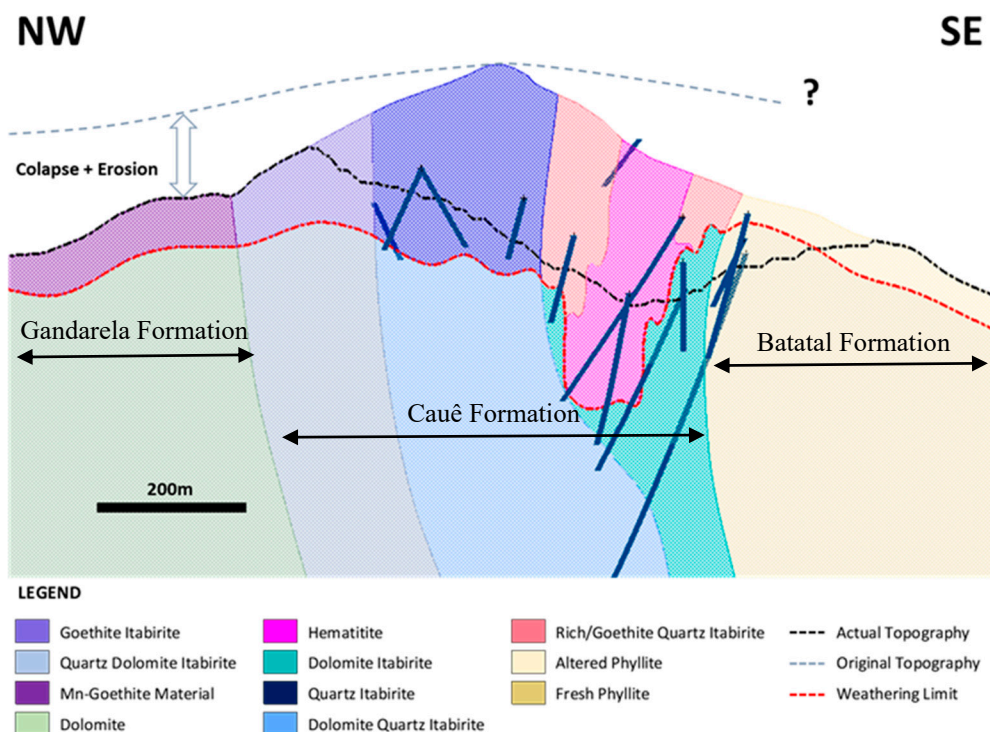


**Figure 18.** Vertical Section of an Iron Deposit of VALE.

Figure 18 illustrates the application of the above concepts to a real iron deposit of Vale. As shown in the figure, high-grade supergene ore deposits are developed on the top of dolomite itabirite. The content of iron oxides, quartz, and carbonates in this rock allows the formation of large iron ore deposits. In this particular case, the average Fe grade increased from 33 wt. % Fe in the protolith to 65 wt. % Fe in the supergene ore (shown as hematite in the figure), with a reduction in the volume of up to 50%, resulting in very Fe-rich and friable iron ore. The rocks that have a higher proportion of carbonates in their composition have more significant leaching potential. However, depending on the amount of iron oxides and Fe-Mn carbonates present in the original rock, they could result in an intermediate to high-grade goethite-Mn oxides ore deposit. Dolomite-quartz itabirites, with an average iron grade of 30%, have a reduced potential for enrichment by leaching because of the low content of carbonates and high grade of quartz. Indeed, the simulations show only 5% of the increase in the average iron grade.

The leaching model illustrated above has been applied during the generation of mineral resource models. It helped to speed up the modeling process and improve the adherence between resource models and grade control models. The leaching model can be upgraded in future studies to incorporate the formation of Mn- and Fe-hydroxides and clay minerals during weathering in the calculations.

## 6. Conclusions

The porosity of hematite-bearing samples can be evaluated by combining direct in situ density test methods, gas pycnometry, and quantitative mineralogical techniques. Methods of direct characterization of mineralogy as XRD and QEMSCAN demonstrated a strong correlation with the indirect normative method MNC, mainly for minerals with higher mass proportion (iron oxi-hydroxides, quartz, and carbonates). The new version of MNC applied to carbonate rocks has shown excellent correlations between mineralogy and density measurements.

The porosity measurements of the weathered itabirites and carbonate rocks, combined with quantitative modal mineralogy, allows a better understanding of the genesis and development of most of the weathered iron ores in the QF and elsewhere. This information

contributes to better define the geological domains, improving the quality of the geological models.

The collapse of the residual matrix in the weathered rock is associated with the leaching of carbonate from the protolith. The higher the original carbonate content of protolith, the bigger the surface depression, matching the geomorphological control of the friable and rich iron deposits verified in the QF region. The leaching model presented herein represents well the reality found in many iron deposits in QF and can be upgraded in future studies, integrating the formation of Mn- and Fe-hydroxides and clay minerals during weathering.

The combination of mineralogical characterization, MNC, and pycnometry represented a low-cost solution, made with the company's own resources, allowing the estimation of mineral paragenesis, density, porosity, and water saturation. Such parameters are critical for the areas of ore process, geotechnics and hydrogeology, not previously considered in resource modeling.

**Author Contributions:** Conceptualization, D.R. and I.M.; methodology R.K.-R. and P.S.; software, I.M. and D.R.; validation, D.B. and C.S.; formal analysis, D.R.; data curation, P.S. and R.K.-R.; writing—original draft preparation, D.R.; writing—review and editing, D.R. and I.M.; visualization, I.M.; supervision, D.R. All authors have read and agreed to the published version of the manuscript.

**Funding:** This research received no external funding.

**Acknowledgments:** Financial support for this study was provided by Vale S.A. We are grateful to Angela Avelar for data generation and discussions, Fernando Machado for the field tests, and Marcia Gomes and all workmates that indirectly contributed to this work.

**Conflicts of Interest:** The authors declare no conflict of interest.

## Appendix A

**Table A1.** Original weathered sample data with lithology, chemical grades, bulk density, moisture, and mineral density (PYC) measurements and calculated mineral proportions, mineral density (CNM), porosity (CNM and PYC), and saturation (CNM and PYC).

Sample	Litho	U (%)	Ps (g/cm³)	Fe (%)	SiO₂ (%)	P (%)	Al₂O₃ (%)	Mn (%)	LOI (%)	TiO₂ (%)	MgO (%)	CaO (%)	FeO (%)	Clo_Oxi	Ap (%)	Wav (%)	Kln (%)	Gbs (%)	Tlc (%)	Qz (%)	MnO (%)	Mag (%)	Gth (%)	Hem (%)	Clo_Min	ρ_MNC (g/cm³)	ρ_PYC (g/cm³)	φ_MNC (%)	φ_PYC (%)	φs_MNC (%)	φs_PYC (%)
ABO-DE000080	IMN	5.10	3.49	66.69	1.41	0.05	0.98	0.45	2.28	0.03	0.02	0.02	0.18	100.75	0.02	0.17	2.29	0.00	0.07	0.30	0.59	0.58	21.02	75.87	100.91	4.91	4.92	28.83	29.04	65.08	64.62
ABO-DE000084	IMN	6.10	3.06	57.28	2.68	0.08	1.45	7.10	4.29	0.03	0.02	0.02	0.18	99.72	0.03	0.30	3.34	0.00	0.06	1.09	9.16	0.58	40.88	44.57	100.02	4.60	4.77	33.54	35.82	59.25	55.49
ABO-DE000085	IMN	12.70	2.46	45.30	8.38	0.05	4.10	10.73	7.56	0.13	0.18	0.08	0.20	99.15	0.12	0.14	10.22	0.00	0.56	3.27	13.85	0.64	72.93	0.00	101.73	4.04	4.16	39.07	40.80	91.59	87.71
ABO-DE000087	IMN	15.70	2.33	44.90	11.84	0.07	1.51	11.49	6.43	0.07	0.07	0.01	0.18	99.09	0.00	0.28	3.52	0.00	0.23	10.06	14.84	0.58	61.97	7.90	99.37	4.09	4.25	43.01	45.10	101.04	96.37
ABO-DE000090	IMN	9.60	2.54	50.65	6.26	0.06	4.44	6.19	8.01	0.16	0.07	0.03	0.18	99.49	0.04	0.23	11.01	0.00	0.21	1.00	7.99	0.58	77.54	2.13	100.73	4.07	4.23	37.61	39.95	71.73	67.53
ABO-DE000091	IMN	9.70	2.26	39.59	32.94	0.04	2.68	2.68	3.83	0.07	0.02	0.01	0.29	99.68	0.02	0.14	6.65	0.00	0.07	29.80	3.46	0.94	36.36	22.96	100.40	3.65	3.68	38.14	38.58	63.63	62.91
ABO-DE000095	IMN	2.40	2.75	42.57	7.37	0.07	2.91	14.29	8.02	0.13	0.17	0.09	0.18	98.12	0.13	0.19	7.16	0.00	0.54	3.70	18.44	0.58	77.42	0.00	108.16	4.13	4.24	33.48	35.10	20.19	19.25
ABO-DE000097	IFR	3.80	2.69	52.38	23.20	0.02	1.00	0.12	0.62	0.02	0.01	0.01	0.18	99.93	0.01	0.07	2.47	0.00	0.04	22.02	1.05	0.58	4.75	70.03	100.12	4.20	4.20	35.97	35.97	29.52	29.52
ABO-DE000100	IMN	6.10	2.90	50.45	23.66	0.04	1.56	0.67	1.48	0.06	0.01	0.01	0.18	99.83	0.01	0.14	3.79	0.00	0.04	21.86	0.86	0.58	13.21	59.67	100.18	4.10	4.06	29.21	28.56	64.52	65.98
ABO-DE000104	IMN	8.10	2.48	56.90	7.20	0.05	2.38	2.71	5.35	0.08	0.04	0.02	0.18	100.00	0.03	0.19	5.81	0.00	0.12	4.41	3.50	0.58	51.28	34.67	100.60	4.33	4.33	42.66	51.34	51.36	51.36
ABO-DE000107	IF	9.50	2.23	49.21	28.07	0.02	1.36	0.08	1.01	0.03	0.02	0.01	1.13	100.88	0.02	0.06	3.37	0.00	0.07	26.45	0.10	3.65	8.58	58.87	101.19	4.01	4.04	44.44	44.83	52.65	52.20
ABO-DE000147	IF	10.80	2.86	58.41	0.53	0.06	4.82	0.05	5.42	0.32	0.03	0.01	0.18	93.39	0.01	0.23	1.01	0.61	0.10	0.00	0.58	29.48	56.44	94.52	4.43	4.73	35.32	39.46	98.16	87.85	
ABO-DE000172	HF	5.40	3.03	63.05	2.26	0.04	0.86	3.50	1.79	0.03	0.01	0.02	0.18	99.71	0.03	0.13	2.05	0.00	0.04	1.28	4.52	0.58	16.24	74.97	99.84	4.90	4.97	38.19	39.12	45.24	44.17
ABO-DE000174	HF	10.40	2.83	65.70	1.05	0.02	0.49	2.07	1.14	0.01	0.01	0.01	0.18	99.34	0.02	0.08	1.15	0.00	0.04	2.67	0.58	9.82	84.52	99.36	5.05	5.12	44.04	44.79	74.50	73.26	
ABO-DE000175	IFR	4.90	3.71	63.20	8.61	0.03	0.81	0.01	0.71	0.06	0.01	0.00	0.31	100.62	0.00	0.11	1.94	0.00	0.04	7.68	0.02	1.01	5.57	84.32	100.71	4.75	4.76	21.75	88.02	87.15	87.15
ABO-DE000176	IFR	4.20	3.09	63.74	7.38	0.03	1.00	0.01	0.84	0.03	0.01	0.00	0.26	100.44	0.00	0.10	2.43	0.00	0.04	6.22	0.01	0.83	6.85	84.14	100.63	4.78	4.76	35.17	38.22	38.46	38.46
ABO-DE000177	IFR	4.60	3.29	66.72	3.79	0.02	0.55	0.04	0.58	0.01	0.01	0.00	0.18	100.42	0.01	0.08	1.30	0.00	0.04	3.16	0.05	0.58	4.29	90.96	100.47	4.99	4.91	34.13	31.69	46.41	49.99
ABO-DE000178	IFR	6.50	2.99	66.36	1.64	0.02	2.18	0.01	1.65	0.01	0.01	0.00	0.26	100.43	0.00	0.08	3.47	1.20	0.04	0.00	0.82	0.85	7.43	100.43	4.91	4.82	39.18	38.00	53.02	54.66	
ABO-DE000179	IFR	8.40	2.66	58.81	9.59	0.02	3.77	0.02	1.93	0.07	0.01	0.00	0.22	99.50	0.00	0.08	9.45	0.00	0.04	5.17	0.02	0.70	17.62	67.54	100.63	4.44	4.48	40.15	40.64	60.74	60.00
ABO-DE000180	IFR	5.70	2.85	66.67	3.44	0.02	0.63	0.01	0.50	0.03	0.01	0.00	0.30	99.96	0.00	0.08	1.50	0.00	0.04	2.72	0.01	0.95	3.56	91.14	100.02	5.00	4.92	43.08	42.10	39.97	40.90
ABO-FD00008-073	IC	3.23	26.91	59.75	0.02	0.18	0.01	0.22	0.01	0.04	0.02	0.00	0.88	98.65	0.03	0.04	0.41	0.00	0.13	59.48	0.02	2.84	0.72	34.90	98.57	3.28	3.31	1.60	2.43		
ABO-FD00008-074	IC	3.09	21.63	66.78	0.01	0.38	0.02	0.27	0.01	0.05	0.01	0.01	0.80	98.39	0.02	0.04	0.92	0.00	0.16	66.25	0.02	2.58	1.20	27.18	98.37	3.13	3.19	1.28	2.98		
ABO-FD00008-077	IC	3.16	31.33	54.84	0.01	0.30	0.04	0.22	0.01	0.03	0.01	0.00	1.05	100.16	0.02	0.03	0.73	0.00	0.11	54.43	0.05	3.48	0.74	40.54	100.12	3.40	3.44	6.98	8.03		
ABO-FD00008-083	IC	3.64	41.34	40.63	0.01	0.19	0.02	0.17	0.01	0.07	0.01	0.01	0.55	100.17	0.02	0.03	0.45	0.00	0.22	40.28	0.02	1.77	0.19	57.11	100.09	3.75	3.74	2.96	2.75		
ABO-FD00008-089	IC	2.76	36.19	47.91	0.01	0.22	0.01	0.18	0.02	0.01	0.02	0.00	0.77	100.05	0.03	0.02	0.53	0.00	0.03	47.64	0.01	2.48	0.37	48.85	99.97	3.56	3.55	22.43	22.16		
ABO-FD00011-046	IC	3.20	34.21	49.65	0.01	0.13	0.01	0.27	0.01	0.01	0.02	0.00	0.46	98.99	0.03	0.03	0.30	0.00	0.03	49.49	0.01	1.48	1.26	46.25	98.89	3.51	3.52	8.64	8.96		
ABO-FD00011-056	IC	3.36	35.86	47.16	0.04	0.36	0.01	0.26	0.01	0.01	0.01	0.00	0.97	99.08	0.02	0.16	0.75	0.00	0.03	46.79	0.01	3.13	1.17	47.00	99.04	3.56	3.55	5.57	5.41		
ABO-FD00018-041	IC	3.31	35.01	48.95	0.01	0.26	0.01	0.19	0.01	0.09	0.01	0.01	0.65	99.53	0.02	0.03	0.63	0.00	0.02	29.48	0.01	2.09	0.36	47.58	99.48	3.53	3.44	6.18	3.76		
ABO-FD00018-042	IC	3.12	30.78	54.85	0.03	0.20	0.01	0.43	0.01	0.01	0.01	0.01	0.90	99.50	0.02	0.10	0.40	0.00	0.03	54.64	0.01	2.90	2.84	38.46	99.41	3.39	3.41	7.99	8.64		
ABO-FD00018-043	IC	3.07	32.56	52.30	0.04	0.20	0.01	0.42	0.02	0.02	0.01	0.01	0.64	99.55	0.02	0.14	0.35	0.00	0.05	52.11	0.01	2.06	2.74	41.97	99.45	3.44	3.43	10.79	10.42		
ABO-FD00018-045	IC	3.32	32.49	53.05	0.01	0.22	0.01	0.22	0.01	0.01	0.01	0.01	0.71	99.93	0.02	0.04	0.52	0.00	0.03	52.79	0.01	2.29	0.77	43.40	99.87	3.44	3.44	3.51	3.51		
ABO-FD00018-046	IC	3.10	29.23	58.26	0.01	0.13	0.01	0.23	0.01	0.03	0.02	0.03	0.93	100.40	0.03	0.02	0.30	0.00	0.08	58.07	0.01	3.00	0.84	37.94	100.30	3.34	3.33	7.15	6.92		
ABO-FD00018-048	IC	3.16	27.29	60.63	0.01	0.22	0.01	0.35	0.01	0.04	0.06	0.05	0.75	100.27	0.00	0.00	0.00	0.00	0.00	60.63	0.01	2.42	3.45	33.42	99.93	3.28	3.45	3.58	8.40		
ABO-FD00018-049	IC	3.57	39.75	42.97	0.01	0.10	0.01	0.11	0.01	0.01	0.01	0.01	0.58	100.01	0.02	0.03	0.22	0.00	0.03	42.85	0.01	1.87	0.00	55.19	100.22	3.69	3.69	3.44			

Table A1. Cont.

Sample	Litho	U (%)	Ps (g/cm³)	Fe (%)	SiO₂ (%)	P (%)	Al₂O₃ (%)	Mn (%)	LOI (%)	TiO₂ (%)	MgO (%)	CaO (%)	FeO (%)	Clo_Oxi	Ap (%)	Wav (%)	Kln (%)	Gbs (%)	Tlc (%)	Qz (%)	MnO (%)	Mag (%)	Gth (%)	Hem (%)	Clo_Min	ρ_MNC (g/cm³)	ρ_PYC (g/cm³)	φ_MNC (%)	φ_PYC (%)	φs_MNC (%)	φs_PYC (%)
CCE-DE000084	IF	4.91	2.89	58.17	15.71	0.02	0.14	0.00	0.20	0.00	0.01	0.00	0.23	99.25	0.00	0.06	0.30	0.00	0.04	15.54	0.00	0.75	0.55	81.91	99.17	4.53	4.55	36.24	41.21	41.02	
CCE-DE000086	IF	3.04	2.60	45.76	32.28	0.03	1.51	0.01	0.75	0.04	0.01	0.00	0.19	100.07	0.00	0.10	3.73	0.00	0.04	30.51	0.02	0.61	6.01	59.41	100.43	3.89	3.90	33.10	33.23	24.67	24.58
CCE-DE000107	IMN	1.65	2.80	51.71	24.24	0.01	0.07	1.19	0.44	0.01	0.01	0.02	0.18	100.25	0.02	0.03	0.13	0.00	0.04	24.15	1.53	0.58	2.92	70.72	100.13	4.22	4.28	33.47	34.51	14.06	13.64
CCE-DE000108	IF	1.19	2.62	39.37	44.01	0.01	0.09	0.00	0.15	0.01	0.01	0.00	0.20	100.56	0.00	0.02	0.21	0.00	0.04	43.89	0.00	0.63	0.09	55.56	100.45	3.67	3.69	28.51	28.90	11.08	10.93
CCE-DE000153	IF	1.37	2.84	50.69	26.32	0.01	0.10	0.00	0.28	0.01	0.01	0.01	0.18	99.19	0.01	0.02	0.23	0.00	0.04	26.18	0.01	0.58	1.36	70.66	99.08	4.15	4.21	31.58	32.49	12.50	12.15
CCE-DE000160	IF	1.89	2.60	51.30	25.93	0.01	0.23	0.07	0.28	0.02	0.01	0.00	0.18	99.91	0.01	0.04	0.53	0.00	0.04	25.65	0.08	0.58	1.40	71.50	99.84	4.17	4.16	37.72	37.66	13.25	13.28
CCE-DE000161	IF	2.49	2.58	44.97	35.96	0.01	0.10	0.00	0.23	0.01	0.01	0.01	0.18	100.62	0.01	0.03	0.23	0.00	0.04	35.82	0.01	0.58	0.83	62.97	100.51	3.88	3.88	33.59	33.61	19.58	19.57
CCE-DE000171	IF	1.52	2.90	44.70	35.57	0.01	0.08	0.00	0.22	0.00	0.01	0.00	0.25	99.78	0.01	0.03	0.17	0.00	0.04	35.47	0.00	0.80	0.72	62.44	99.67	3.88	3.91	25.34	25.80	17.66	17.34
CCE-DE000183	IF	2.57	2.99	45.78	35.08	0.01	0.13	0.00	0.19	0.00	0.01	0.01	0.25	100.85	0.01	0.02	0.30	0.00	0.04	34.91	0.00	0.79	0.47	64.21	100.76	3.91	4.19	23.58	23.89	33.40	27.46
CCE-DE000184	IF	1.47	3.06	52.58	25.15	0.01	0.01	0.13	0.00	0.01	0.01	0.01	0.28	100.48	0.01	0.02	0.00	0.00	0.04	25.12	0.02	0.89	0.00	74.39	100.49	4.22	4.23	27.44	27.72	16.64	16.47
CMT-DE000074	IAL	9.40	2.37	30.38	50.97	0.09	3.51	0.01	2.06	0.31	0.07	0.01	0.26	100.56	0.02	0.35	8.51	0.00	0.21	46.88	0.02	0.83	18.83	25.66	101.30	3.32	3.39	28.45	29.94	86.53	82.22
CMT-DE000075	IF	6.40	2.18	35.49	47.74	0.04	1.14	0.01	0.86	0.03	0.04	0.01	0.44	100.61	0.02	0.13	2.75	0.00	0.13	46.37	0.01	1.42	7.05	42.95	100.83	3.51	3.57	37.80	38.77	39.50	38.51
CMT-DE000076	IFR	5.00	2.90	53.54	22.82	0.02	0.71	0.00	0.50	0.04	0.02	0.01	0.24	100.67	0.01	0.06	1.73	0.00	0.06	21.98	0.00	0.77	3.56	72.57	100.74	4.24	4.30	31.48	32.53	48.56	46.99
CMT-DE000077	IF	8.40	2.48	42.92	36.66	0.03	1.16	0.00	0.70	0.08	0.03	0.01	0.44	100.02	0.02	0.09	2.85	0.00	0.10	35.27	0.00	1.41	5.42	55.04	100.21	3.79	3.85	34.61	35.66	65.60	63.67
CMT-DE000079	IF	5.90	2.68	40.43	39.80	0.04	1.50	0.00	1.53	0.09	0.03	0.01	0.20	100.83	0.01	0.16	3.62	0.00	0.11	38.04	0.00	0.64	13.70	44.83	101.12	3.66	3.72	26.87	28.07	62.43	59.75
CMT-DE000080	IFR	4.90	3.07	56.43	17.87	0.03	1.10	0.00	0.87	0.07	0.02	0.01	0.32	100.66	0.02	0.12	2.66	0.00	0.06	16.60	0.01	1.02	7.12	73.24	100.84	4.36	4.46	29.61	31.16	53.44	50.78
CMT-DE000082	IF	6.40	2.81	36.72	43.57	0.05	2.04	0.00	1.20	0.09	0.05	0.01	0.20	99.54	0.01	0.17	4.97	0.00	0.15	41.16	0.00	0.63	10.39	42.52	100.01	3.55	3.60	20.75	21.89	92.75	87.93
CMT-DE000083	IF	4.50	2.72	46.58	30.86	0.02	1.43	0.00	0.76	0.08	0.03	0.01	0.37	99.77	0.01	0.08	3.53	0.00	0.08	29.16	0.00	1.19	6.07	59.93	100.06	3.93	3.99	30.76	31.74	41.70	40.41
CMT-DE000084	IF	4.40	2.79	39.49	43.39	0.02	0.55	0.00	0.33	0.04	0.03	0.02	0.18	100.83	0.03	0.05	1.34	0.00	0.10	42.70	0.00	0.59	1.80	54.24	100.85	3.66	3.71	24.74	24.84	54.08	51.96
CMT-DE000087	HF	6.89	2.67	64.40	2.58	0.06	2.15	0.11	2.44	0.07	0.08	0.01	3.11	99.32	0.02	0.21	5.19	0.03	0.25	0.00	0.14	10.03	16.73	66.67	99.27	4.80	4.85	44.35	44.86	44.60	44.10
CMT-DE000088	HF	7.90	2.67	65.68	2.49	0.03	1.55	0.13	1.81	0.05	0.08	0.02	0.69	100.05	0.03	0.11	3.82	0.00	0.24	0.56	0.16	2.21	16.33	76.95	100.41	4.86	4.97	45.05	46.19	50.87	49.62
CMT-DE000089	IFR	6.09	2.63	53.51	19.49	0.03	1.22	0.75	1.15	0.02	0.07	0.01	2.17	99.25	0.02	0.10	2.98	0.00	0.22	17.96	0.02	0.70	9.83	60.44	99.52	4.26	4.34	38.40	39.49	44.35	43.12
CMT-DE000090	IF	11.23	1.99	40.09	36.61	0.07	1.86	0.16	2.82	0.15	0.15	0.02	0.51	99.23	0.02	0.26	4.43	0.00	0.47	34.25	0.21	1.65	26.23	32.05	99.57	3.64	3.72	45.18	46.37	55.82	54.39
CMT-DE000092	IF	6.84	2.56	44.60	34.08	0.02	0.57	0.07	0.73	0.03	0.05	0.01	0.37	99.34	0.02	0.08	1.34	0.00	0.14	33.07	0.09	1.19	5.76	57.37	99.36	3.87	3.98	33.95	35.80	55.29	52.43
CMT-DE000093	IF	4.47	2.62	45.35	34.69	0.08	0.15	0.11	0.95	0.02	0.03	0.01	0.65	100.95	0.05	0.27	0.09	0.00	0.08	34.60	0.14	2.08	7.95	55.55	100.82	3.87	3.93	32.33	33.89	36.68	36.68
CMT-DE000094	IF	6.93	2.71	39.90	41.03	0.07	0.10	0.29	1.30	0.01	0.03	0.03	0.37	100.03	0.04	0.24	0.00	0.00	0.10	40.97	0.37	1.18	11.37	45.62	99.89	3.67	3.73	26.30	27.43	76.66	73.49
CMT-DE000095	IF	4.47	2.66	36.76	44.89	0.06	0.24	0.24	0.98	0.01	0.04	0.02	0.18	99.16	0.03	0.23	0.37	0.00	0.11	44.64	0.31	0.58	8.21	44.58	99.07	3.58	3.64	25.77	26.91	48.26	46.21
CMT-DE000096	IF	5.14	2.57	43.25	33.20	0.02	2.54	0.01	1.34	0.01	0.04	0.01	0.18	99.01	0.02	0.06	6.36	0.00	0.13	30.16	0.01	0.58	11.74	50.69	99.75	3.79	3.87	32.06	33.47	43.48	41.64
CMT-DE000097	IFR	3.90	2.94	55.50	17.35	0.03	1.71	0.00	0.95	0.11	0.03	0.02	0.68	99.51	0.03	0.10	4.21	0.00	0.10	15.32	0.00	2.19	7.94	69.97	99.86	4.34	4.47	32.29	34.29	36.90	34.75
CMT-DE000098	IF	3.44	2.73	30.82	53.53	0.03	1.10	0.00	0.72	0.04	0.01	0.01	0.30	99.50	0.01	0.10	2.68	0.00	0.04	52.25	0.00	0.98	5.69	57.94	99.71	3.50	3.50	19.19	21.95	50.69	44.30
CMT-DE000099	HF	8.16	2.96	66.17	1.20	0.14	1.30	0.02	0.57	0.04	0.05	0.02	0.18	99.12	0.03	0.05	2.36	0.23	0.15	0.00	0.03	0.58	11.33	83.84	99.08	4.96	5.00	40.42	40.85	65.00	64.33
CMT-DE000100	IFR	7.54	2.84	57.60	13.78	0.11	1.23	0.00	1.73	0.03	0.04	0.02	0.18	99.42	0.03	0.11	2.69	0.00	0.13	12.45	0.01	0.58	15.63	67.72	99.64	4.42	4.45	35.84	36.19	64.56	63.94
CMT-DE000101	IFR	6.66	2.79	56.34	17.94	0.03	0.65	0.00	0.66	0.01	0.01	0.02	0.70	99.88	0.03	0.12	1.51	0.00	0.14	17.20	0.00	2.26	5.07	73.67	99.91	4.39	4.51	36.45	38.17	54.64	52.17
CMT-DE000102	HF	5.58	3.15	66.65	2.25	0.07	1.26	0.01	1.10	0.07	0.01	0.02	0.77	100.07	0.03	0.25	2.92	0.00	0.04	0.86	0.01	2.48	9.40	84.29	100.29</td						

**Table A1.** Cont.

Sample	Litho	U (%)	Ps (g/cm³)	Fe (%)	SiO₂ (%)	P (%)	Al₂O₃ (%)	Mn (%)	LOI (%)	TiO₂ (%)	MgO (%)	CaO (%)	FeO (%)	Clo_Oxi	Ap (%)	Wav (%)	Kln (%)	Gbs (%)	Tlc (%)	Qz (%)	MnO (%)	Mag (%)	Gth (%)	Hem (%)	Clo_Min	ρ_MNC (g/cm³)	ρ_PYC (g/cm³)	φ_MNC (%)	φ_PYC (%)	φs_MNC (%)	φs_PYC (%)
CMT-DE000134	IFR	3.82	2.83	52.34	23.16	0.02	0.92	0.00	0.75	0.03	0.05	0.04	0.18	99.80	0.05	0.06	2.27	0.00	0.14	22.01	0.00	0.58	5.89	68.95	99.97	4.19	4.28	32.41	33.84	34.72	33.26
CMT-DE000135	HF	7.05	3.20	65.81	2.35	0.03	1.92	0.02	1.07	0.04	0.02	0.03	0.18	99.59	0.05	0.11	4.75	0.00	0.07	0.09	0.02	0.58	9.08	85.35	100.09	4.91	5.03	34.79	36.30	69.88	66.97
CMT-DE000136	IF	10.78	2.11	44.94	31.52	0.04	1.03	0.15	1.79	0.05	0.14	0.03	0.18	99.06	0.05	0.11	2.49	0.00	0.43	30.09	0.19	0.58	16.08	49.22	99.23	3.86	3.93	45.43	46.42	56.00	54.81
GAL-FSD-02-0001-001DE	IC	3.32	33.14	52.95	0.01	0.20	0.00	0.17	0.00	0.01	0.01	0.31	100.71	0.01	0.03	0.47	0.00	0.04	52.70	0.00	1.01	0.30	46.08	100.64	3.46	3.51	3.84	5.33			
GAL-FSD-02-0001-003DE	IC	3.82	43.14	38.65	0.01	0.18	0.00	0.14	0.00	0.04	0.00	0.46	100.67	0.01	0.04	0.41	0.00	0.13	38.37	0.00	1.49	0.00	60.20	100.65	3.81	3.75	-0.40	-1.93			
GAL-FSD-03-0027-001DE	IC	3.21	34.35	49.77	0.05	0.13	0.03	2.24	0.00	0.01	0.00	4.03	100.95	0.00	0.18	0.13	0.00	0.04	49.69	0.03	12.98	20.65	17.13	100.83	3.43	3.38	6.38	4.96			
GAL-FSD-03-0028-001DE	IC	2.95	35.65	44.10	0.02	0.11	0.00	4.81	0.00	0.01	0.01	0.31	100.03	0.01	0.08	0.20	0.00	0.04	43.98	0.00	0.98	46.01	8.62	99.92	3.44	3.44	14.17	14.28			
GAL-FSD-03-0033-001DE	IC	3.04	32.59	51.44	0.04	0.15	0.02	2.11	0.00	0.04	0.01	0.66	100.38	0.01	0.14	0.22	0.00	0.11	51.27	0.03	2.12	19.37	27.01	100.28	3.40	3.42	10.62	11.22			
GAL-FSD-03-0041-001DE	IC	3.05	33.38	48.15	0.02	0.12	0.00	3.57	0.00	0.01	0.00	0.60	99.56	0.00	0.07	0.22	0.00	0.04	48.03	0.00	1.94	33.79	15.35	99.45	3.40	3.34	10.15	8.63			
GAL-FSD-04-0011-003DE	IC	4.99	67.80	1.02	0.05	0.68	0.02	0.41	0.04	0.01	0.03	0.37	99.21	0.04	0.18	1.53	0.00	0.04	0.28	0.02	1.18	2.61	93.38	99.27	5.12	5.29	2.49	5.59			
GAL-FSD-04-0012-001DE	HC	3.49	43.46	33.13	0.07	0.04	0.04	3.69	0.00	0.04	0.01	0.88	99.15	0.02	0.25	0.00	0.00	0.14	33.12	0.05	2.82	34.96	27.80	99.16	3.74	3.63	6.63	3.76			
GAL-FSD-04-0022-002DE	IC	3.35	31.47	52.57	0.04	0.08	0.02	2.16	0.00	0.03	0.01	0.64	99.89	0.01	0.16	0.02	0.00	0.10	52.49	0.03	2.05	19.89	25.01	99.76	3.37	3.37	0.50	0.61			
GAL-FSD-04-0030-001DE	IC	2.98	40.61	40.45	0.03	0.22	0.03	1.09	0.00	0.13	0.01	1.32	99.89	0.01	0.10	0.44	0.00	0.41	39.98	0.04	4.25	9.14	45.46	99.82	3.70	3.54	19.33	15.79			
GAL-FSD-04-0030-002DE	IC	3.29	48.12	28.24	0.05	0.27	0.01	2.07	0.02	0.07	0.00	0.82	99.52	0.00	0.21	0.47	0.00	0.21	27.89	0.02	2.65	18.89	49.09	99.43	3.97	3.94	17.22	16.59			
GAL-FSD-04-0030-003DE	IC	3.57	38.13	41.62	0.08	0.07	0.01	4.15	0.00	0.05	0.05	2.76	100.33	0.08	0.26	0.00	0.00	0.15	41.57	0.01	8.91	39.47	9.83	100.28	3.52	3.37	-1.59	-6.06			
GAL-FSD-04-0031-002DE	IC	3.46	48.66	29.61	0.01	0.28	0.01	0.26	0.01	0.05	0.00	0.61	99.73	0.00	0.04	0.66	0.00	0.14	29.21	0.01	1.97	1.08	66.57	99.70	4.05	4.06	14.44	14.72			
GAL-FSD-04-0031-004DE	IC	4.62	66.65	2.60	0.03	0.68	0.02	0.39	0.05	0.04	0.04	0.46	99.14	0.06	0.08	1.63	0.00	0.12	1.77	0.03	1.47	2.39	91.65	99.19	5.05	5.11	8.47	9.58			
GAL-FSD-04-0036-003DE	IC	5.02	64.82	6.88	0.14	0.32	0.01	0.36	0.02	0.03	0.17	1.46	100.63	0.27	0.40	0.38	0.00	0.08	6.65	0.02	4.70	2.01	86.03	100.54	4.86	4.88	-3.13	-2.80			
GAL-FSD-04-0036-008DE	HC	5.25	69.09	0.55	0.02	0.15	0.01	0.12	0.00	0.01	0.03	0.63	99.63	0.04	0.06	0.32	0.00	0.04	0.38	0.01	2.04	0.00	96.87	99.76	5.21	5.33	-0.60	1.58			
GAL-FSD-04-0045-001DE	HC	3.38	27.68	60.33	0.05	0.09	0.00	0.15	0.00	0.02	0.12	0.40	100.36	0.18	0.11	0.11	0.00	0.05	60.24	0.00	1.30	0.00	38.27	100.27	3.30	3.26	-2.41	-3.53			
JGD-FD00001-037	HC	4.63	66.38	5.17	0.09	0.31	0.01	0.58	0.04	0.51	0.40	0.10	102.14	0.62	0.02	0.76	0.00	1.61	3.80	0.01	0.32	3.30	91.63	102.07	4.92	4.84	5.89	4.39			
JGD-FD00001-038	HC	4.32	67.07	2.00	0.15	0.19	0.02	1.05	0.02	0.21	0.51	0.10	100.24	0.81	0.14	0.33	0.00	0.66	1.43	0.03	0.32	8.35	88.06	100.13	5.02	4.96	13.91	12.90			
JGD-FD00005-054	HC	4.73	69.86	1.80	0.10	0.07	0.00	0.23	0.03	0.43	0.40	0.10	103.08	0.63	0.06	0.12	0.00	1.34	0.90	0.00	0.32	0.03	99.54	102.94	5.12	5.07	7.61	6.66			
JGD-FD00013-042	HC	4.83	67.28	2.21	0.10	0.95	0.03	0.76	0.05	0.91	0.65	0.10	101.98	0.00	0.00	0.00	0.00	0.21	0.03	0.32	7.54	89.10	99.20	5.07	5.01	4.75	3.61				
JGD-FD00014-046	HC	4.89	69.01	1.39	0.09	0.07	0.01	0.26	0.02	0.15	0.33	0.10	101.11	0.52	0.06	0.11	0.00	0.47	1.04	0.01	0.32	0.74	97.69	100.97	5.15	5.15	5.09	5.08			
JGD-FD00014-054	HC	4.34	67.24	1.19	0.08	0.63	0.02	0.68	0.05	0.32	0.38	0.10	99.58	0.00	0.00	0.00	0.19	0.03	0.32	6.67	89.83	98.04	5.13	5.10	15.42	15.02					
JGD-FD00015-058	HC	4.65	66.07	2.95	0.05	0.88	0.02	0.33	0.06	1.14	0.10	0.10	100.04	0.15	0.10	1.49	0.38	3.56	0.00	0.03	0.32	0.00	95.77	101.80	4.99	4.99	6.83	6.92			
JGD-FD00030-039	IC	3.06	43.78	36.41	0.01	0.09	0.01	0.96	0.01	0.11	0.15	0.10	100.35	0.00	0.00	0.00	0.00	0.41	0.01	0.32	9.46	53.76	99.97	3.82	3.75	19.73	18.19				
JGD-FD00030-040	IC	3.14	38.88	43.64	0.01	0.28	0.01	0.95	0.01	0.09	0.08	0.10	100.68	0.00	0.00	0.00	0.00	43.64	0.02	0.32	9.40	46.81	100.19	3.63	3.59	13.55	12.42				
JGD-FD00030-041	IC	2.77	30.34	54.76	0.04	0.20	0.01	1.35	0.00	0.11	0.06	0.10	99.96	0.09	0.11	0.39	0.00	0.36	54.35	0.01	0.32	11.72	32.52	99.87	3.35	3.37	17.27	17.71			
JGD-FD00030-042	IC	2.82	32.28	51.71	0.05	0.16	0.02	1.27	0.01	0.10	0.13	0.10	99.66	0.20	0.09	0.31	0.00	0.31	51.38	0.03	0.32	10.94	35.99	99.55	3.42	3.36	17.39	16.08			
JGD-FD00035-033	IC	3.57	42.27	38.14	0.20	0.12	0.00	0.25	0.01	0.10	0.81	0.10	100.34	1.28	0.08	0.22	0.00	0.30	37.85	0.00	0.32	0.47	59.70	100.22	3.79	3.82	5.89	6.51			
JGD-FD00035-034	IC	3.69	44.05	35.43	0.06	0.12	0.01	0.09	0.01	0.11	0.56	0.10	99.45	0.00	0.00	0.00	0.00	35.43	0.01	0.32	0.93	61.82	98.51	3.88	3.84	4.80	3.73				
JGD-FD00036-057	IC	3.40	47.33	31.77	0.01	0.20	0.04	0.10	0.03	0.04	0.04	0.10	99.92	0.06	0.02	0.48	0.00	0.14	31.46	0.05	0.32	0.00	67.81	100.34	4.00	3.97	15.04	14.39			
JGD-FD00036-062	IC	3.21	33.10	52.74	0.08	0.05	0.00	0.56	0.01	0.13	0.70	0.10	101.75	0.00	0.00	0.00	0.00	52.74	0.00	0.32	5.55	42.01	100.63	3.44	3.45	6.76	7.01				
JGD-FD00036-065	HC	4.82	69.66	1.92	0.07	0.11	0.02	0.55	0.03	0.37	0.59	0.10	103.34	0.00	0.00	0.00	0.00	1.92	0.02	0.32	5.45	94.37	102.09	5.11	5.08	5.72</td					

**Table A1.** Cont.

Sample	Litho	U (%)	Ps (g/cm³)	Fe (%)	SiO₂ (%)	P (%)	Al₂O₃ (%)	Mn (%)	LOI (%)	TiO₂ (%)	MgO (%)	CaO (%)	FeO (%)	Clo_Oxi	Ap (%)	Wav (%)	Kln (%)	Gbs (%)	Tlc (%)	Qz (%)	MnO (%)	Mag (%)	Gth (%)	Hem (%)	Clo_Min	ρ_MNC (g/cm³)	ρ_PYC (g/cm³)	φ_MNC (%)	φ_PYC (%)	φs_MNC (%)	φs_PYC (%)
JPE-DE000069	IC	2.87	30.25	56.64	0.01	0.08	0.00	0.22	0.00	0.04	0.02	0.61	100.22	0.03	0.04	0.16	0.00	0.13	56.49	0.00	1.98	0.71	40.58	100.11	3.37	3.41	14.92	15.88			
JPE-DE000071	IC	3.10	35.63	49.10	0.01	0.38	0.01	0.30	0.00	0.03	0.00	0.27	100.76	0.00	0.04	0.92	0.00	0.10	48.61	0.01	0.88	1.52	48.68	100.76	3.53	3.59	12.13	13.50			
JPE-DE000072	IC	3.01	29.04	57.82	0.02	0.08	0.00	0.47	0.00	0.01	0.00	0.40	99.92	0.00	0.09	0.11	0.00	0.04	57.75	0.00	1.29	3.26	37.26	99.80	3.33	3.37	9.68	10.82			
JPE-DE000074	IC	3.28	31.66	54.67	0.01	0.10	0.00	0.16	0.00	0.01	0.00	0.40	100.19	0.00	0.02	0.24	0.00	0.04	54.54	0.00	1.27	0.22	43.76	100.09	3.41	3.46	3.93	5.08			
JPE-DE000076	IC	3.25	36.87	47.39	0.01	0.16	0.00	0.13	0.01	0.02	0.01	0.18	100.43	0.01	0.03	0.37	0.00	0.05	47.18	0.00	0.58	0.00	52.21	100.44	3.58	3.63	9.31	10.33			
JPE-DE000077	IC	2.93	29.43	57.77	0.01	0.14	0.01	0.19	0.00	0.03	0.01	0.30	100.22	0.01	0.02	0.33	0.00	0.11	57.55	0.01	0.96	0.43	40.71	100.14	3.35	3.38	12.44	13.39			
JPE-DE000078	IC	3.12	32.94	52.59	0.01	0.11	0.03	0.23	0.00	0.02	0.00	0.28	100.08	0.00	0.02	0.25	0.00	0.07	52.43	0.03	0.89	0.88	45.40	99.99	3.46	3.50	9.75	10.88			
JPE-DE000084	HC	3.26	36.84	46.25	0.07	0.15	0.00	0.18	0.00	0.06	0.20	0.50	99.63	0.31	0.10	0.27	0.00	0.19	46.00	0.01	1.60	0.20	50.85	99.54	3.59	3.65	9.32	10.74			
JPE-DE000085	IC	3.05	28.31	59.38	0.01	0.15	0.00	0.16	0.00	0.06	0.00	0.26	100.22	0.00	0.02	0.35	0.00	0.17	59.11	0.00	0.83	0.07	39.57	100.14	3.31	3.35	7.97	8.90			
JPE-DE000089	HC	4.91	67.72	2.95	0.01	0.36	0.01	0.24	0.02	0.04	0.01	0.34	100.43	0.01	0.03	0.88	0.00	0.13	4.26	0.01	1.09	0.89	94.90	100.41	5.07	5.17	3.14	4.88			
JPE-DE000099	IC	3.59	42.44	38.20	0.05	0.63	0.00	0.42	0.04	0.05	0.07	0.40	100.15	0.11	0.12	1.46	0.00	0.17	37.41	0.00	1.30	2.67	56.94	100.18	3.78	3.83	4.95	6.12			
JPE-DE000092	IC	3.37	33.75	51.28	0.01	0.05	0.02	0.12	0.00	0.03	0.00	0.52	99.72	0.00	0.03	0.09	0.00	0.08	51.18	0.03	1.67	0.00	46.78	99.87	3.49	3.54	3.36	4.66			
JPE-DE000093	IC	3.83	43.91	36.48	0.01	0.04	0.00	0.14	0.00	0.01	0.47	99.43	0.01	0.03	0.07	0.00	0.04	36.42	0.00	1.50	0.00	61.30	99.37	3.86	3.89	0.80	1.67				
JPE-DE000100	IC	3.21	30.17	55.86	0.01	0.07	0.00	0.17	0.00	0.03	0.02	0.36	99.28	0.03	0.04	0.14	0.00	0.10	55.73	0.00	1.15	0.22	41.76	99.16	3.38	3.41	5.10	5.89			
JPE-DE000101	IC	2.88	26.63	60.13	0.01	0.25	0.02	0.51	0.00	0.18	0.17	0.44	99.31	0.00	0.00	0.00	0.00	0.00	60.13	0.02	1.41	5.03	32.09	98.69	3.27	3.31	11.83	13.08			
JPE-DE000102	IC	3.65	50.32	26.54	0.08	0.38	0.01	0.42	0.02	0.16	0.25	0.33	99.85	0.39	0.09	0.86	0.00	0.49	25.82	0.02	1.07	2.42	68.67	99.83	4.12	4.21	11.31	13.28			
JPE-DE000103	IC	3.33	32.54	53.30	0.01	0.06	0.01	0.11	0.00	0.03	0.02	0.36	100.03	0.02	0.03	0.12	0.00	0.08	53.20	0.01	1.17	0.00	45.66	100.29	3.45	3.52	3.40	5.25			
JPE-DE000105	IC	3.31	34.70	49.56	0.01	0.07	0.00	0.17	0.00	0.04	0.03	0.33	99.47	0.04	0.00	0.17	0.00	0.13	49.40	0.00	1.07	0.21	48.33	99.36	3.52	3.59	6.02	7.72			
JPE-DE000107	IC	4.02	55.00	21.22	0.05	0.13	0.01	0.20	0.01	0.02	0.09	0.39	100.36	0.14	0.10	0.22	0.00	0.07	21.07	0.01	1.27	0.48	76.90	100.26	4.34	4.41	7.28	8.90			
JPE-DE000108	IC	3.44	39.95	41.63	0.02	0.29	0.05	0.27	0.01	0.05	0.01	0.40	99.44	0.02	0.08	0.64	0.00	0.14	41.24	0.07	1.28	1.20	54.72	99.40	3.70	3.74	7.20	8.19			
JPE-DE000110	IC	3.24	32.42	52.94	0.02	0.06	0.00	0.12	0.00	0.04	0.01	0.36	99.53	0.02	0.06	0.09	0.00	0.12	52.82	0.00	1.15	0.00	45.39	99.65	3.45	3.51	5.92	7.63			
JPE-DE000111	HC	4.73	68.70	1.10	0.01	0.35	0.01	0.29	0.02	0.01	0.03	0.41	100.00	0.04	0.00	0.88	0.00	0.04	0.66	0.01	1.33	1.45	95.57	99.99	5.16	5.29	8.25	10.57			
JPE-DE000112	HC	4.59	68.97	0.80	0.01	0.21	0.00	0.20	0.02	0.01	0.01	0.26	99.87	0.02	0.04	0.49	0.00	0.04	0.54	0.01	0.84	0.55	97.26	99.80	5.19	5.33	11.63	13.80			
MMI-DE000023	IF	1.52	2.99	47.24	32.18	0.01	0.18	0.00	0.20	0.00	0.01	0.00	0.36	100.10	0.00	0.02	0.43	0.00	0.04	31.95	0.00	0.97	0.53	66.07	100.03	3.98	3.99	24.89	25.05		
MMI-DE000024	IF	0.89	2.91	46.31	33.18	0.01	0.01	0.14	0.00	0.01	0.00	0.26	99.58	0.00	0.02	0.00	0.00	0.04	33.15	0.02	0.85	0.02	65.33	99.45	3.96	3.98	26.46	9.88			
MMI-DE000025	IF	3.11	2.90	53.71	23.37	0.01	0.06	0.15	0.24	0.00	0.01	0.00	0.27	100.67	0.00	0.04	0.12	0.00	0.04	23.28	0.20	0.88	1.00	75.01	100.56	4.27	4.30	32.10	28.98		
MMI-DE000026	IF	3.04	2.91	49.05	29.10	0.01	0.31	0.02	0.26	0.01	0.01	0.00	0.28	99.81	0.00	0.02	0.76	0.00	0.04	28.71	0.02	0.92	1.14	68.17	99.78	4.06	4.09	28.84	31.51		
MMI-DE000039	IF	1.44	2.92	37.81	45.35	0.01	0.29	0.01	0.20	0.01	0.01	0.00	0.19	99.94	0.00	0.02	0.72	0.00	0.04	44.99	0.02	0.61	0.56	52.93	99.91	3.62	3.65	19.42	20.10		
MMI-DE000041	HF	5.38	3.11	65.89	5.11	0.01	0.71	0.18	0.46	0.03	0.01	0.01	0.90	100.70	0.02	0.02	1.78	0.00	0.04	4.26	0.23	2.90	3.13	88.40	100.80	4.93	5.00	36.98	37.95		
MMI-DE000043	HF	3.96	3.44	67.81	3.78	0.00	0.06	0.03	0.12	0.02	0.01	0.00	0.21	100.96	0.00	0.01	0.15	0.00	0.04	3.68	0.03	0.67	0.00	96.51	101.10	5.07	5.12	32.11	43.20		
MMI-DE000044	IF	3.41	2.58	40.26	42.30	0.03	0.16	0.05	0.73	0.01	0.08	0.01	0.53	100.92	0.01	0.11	0.29	0.00	0.04	42.01	0.07	1.70	5.67	100.82	100.82	3.68	3.71	30.05	30.25		
MMI-DE000045	IMN	7.53	2.04	22.77	58.77	0.06	0.15	0.51	3.51	0.21	0.12	0.04	0.07	0.02	0.04	0.18	0.00	0.03	56.89	0.53	0.58	19.45	14.48	100.11	3.19	3.22	36.16	45.92			
MMI-DE000046	IF	2.57	2.60	44.79	36.42	0.00	0.04	0.01	0.08	0.01	0.01	0.00	0.18	100.60	0.00	0.01	0.07	0.00	0.04	36.35	0.01	0.58	0.00	63.96	101.05	3.88	3.91	32.90	33.48		
MMI-DE000047	IF	1.87	2.47	46.34	35.35	0.01	0.03	0.05	0.14	0.01	0.06	0.01	0.26	99.75	0.01	0.01	0.05	0.00	0.19	35.21	0.06	0.83	0.00	63.34	99.70	3.89	3.96	24.59	18.51		
MMI-DE000049	IF	1.66	2.57	34.54	47.81	0.01	1.05	0.04	0.65	0.05	0.02	0.02	0.22	99.04	0.03	0.02	2.64	0.00	0.15	46.48	0.05	0.71	4.94	44.22	99.24	3.51	3.55	26.58	26.75		
MMI-DE000050	IF	2.28	2.54	43.60	35.86	0.01	1.24	0.03	0.70	0.03	0.09	0.02	0.23	100.31	0.03	0.02	3.11	0.00	0.29	34.23	0.04	0.75	5.40	56.72	100.58	3.81	3.86	33.27	34.17		
MMI-DE000051	IF	3.39	2.86	56.85	18.16	0.01	0.06	0.14	0.24	0.01	0.01	0.02	0.26	99.95	0.03	0.01	0.14	0.00	0.04	18.00	0.18	0.85	0.95	79.56	99.83	4.45	4.55	35.79	37.79		
MMI-DE000053	IM																														

**Table A1.** Cont.

Sample	Litho	U (%)	Ps (g/cm³)	Fe (%)	SiO₂ (%)	P (%)	Al₂O₃ (%)	Mn (%)	LOI (%)	TiO₂ (%)	MgO (%)	CaO (%)	FeO (%)	Clo_Oxi	Ap (%)	Wav (%)	Kln (%)	Gbs (%)	Tlc (%)	Qz (%)	MnO (%)	Mag (%)	Gth (%)	Hem (%)	Clo_Min	ρ_MNC (g/cm³)	ρ_PYC (g/cm³)	φ_MNC (%)	φ_PYC (%)	ψs_MNC (%)	ψs_PYC (%)
MMI-DE000122	IF	3.88	2.79	42.18	35.86	0.03	1.13	1.00	0.89	0.01	0.05	0.00	0.18	99.58	0.01	0.11	2.74	0.00	0.15	34.49	1.29	0.58	7.35	53.11	99.82	3.79	3.83	26.46	27.28	42.52	41.25
MMI-DE000123	IF	2.03	2.88	41.96	39.09	0.01	0.85	0.04	0.44	0.01	0.06	0.00	0.18	100.50	0.00	0.04	2.11	0.00	0.17	38.00	0.05	0.58	2.90	56.80	100.65	3.75	3.78	23.16	23.64	25.80	25.28
MMI-DE000141	IF	2.66	2.90	45.63	34.70	0.01	0.04	0.05	0.15	0.00	0.01	0.01	0.18	100.21	0.01	0.03	0.07	0.00	0.04	34.64	0.06	0.58	0.11	64.55	100.09	3.92	3.93	26.02	26.20	30.43	30.22
MMI-DE000142	IF	1.42	3.04	47.16	32.38	0.00	0.03	0.01	0.04	0.00	0.01	0.00	0.18	99.90	0.00	0.01	0.06	0.00	0.04	32.33	0.01	0.58	0.00	67.74	100.78	3.99	4.01	23.99	24.39	18.23	17.93
MMI-DE000144	IF	3.35	2.80	52.72	24.06	0.01	0.08	0.05	0.12	0.00	0.01	0.01	0.18	99.73	0.02	0.02	0.18	0.00	0.04	23.95	0.06	0.58	0.00	74.97	99.82	4.24	4.26	34.00	34.25	28.57	28.36
PIC-FSD-00-0001-002DE	IC	4.42	67.46	1.62	0.02	1.32	0.00	0.77	0.05	0.03	0.03	0.44	100.26	0.05	0.06	3.28	0.00	0.08	0.04	0.01	1.42	6.14	89.47	100.55	5.02	4.96	11.88	10.84			
PIC-FSD-02-0005-001DE	HC	4.82	69.20	0.55	0.04	0.29	0.01	0.16	0.01	0.03	0.09	1.47	100.02	0.14	0.09	0.64	0.00	0.09	0.20	0.01	4.73	0.13	93.94	99.97	5.20	5.24	7.18	7.96			
PIC-FSD-88-0001-002DE	HC	4.87	69.84	0.61	0.02	0.25	0.01	0.19	0.01	0.02	0.03	0.62	100.95	0.05	0.05	0.58	0.00	0.05	0.31	0.01	1.99	0.47	97.40	100.91	5.20	5.23	6.29	6.83			
PIC-FSD-90-0001-001DE	HC	3.20	30.81	56.08	0.04	0.20	0.00	0.13	0.00	0.04	0.07	0.46	100.59	0.11	0.08	0.42	0.00	0.11	55.81	0.00	1.50	0.00	42.69	100.71	3.39	3.30	5.42	2.93			
PIC-FSD-99-0012-001DE	IC	5.03	69.48	0.29	0.03	0.13	0.01	0.11	0.00	0.01	0.07	0.34	99.98	0.11	0.05	0.28	0.00	0.04	0.13	0.01	1.09	0.00	98.52	100.23	5.23	5.32	3.88	5.54			
PIC-FSD-99-0001-001DE	HC	3.44	41.23	40.70	0.01	0.20	0.00	0.20	0.00	0.01	0.01	0.27	100.06	0.01	0.03	0.48	0.00	0.04	40.45	0.00	0.87	0.55	57.56	100.00	3.74	3.76	8.13	8.55			
SEG-DE000063	HC	4.83	69.40	0.30	0.03	0.08	0.01	0.25	0.00	0.09	0.19	0.28	100.18	0.00	0.00	0.00	0.00	0.00	0.30	0.01	0.90	2.44	96.13	99.77	5.22	5.32	7.37	9.08			
SEG-DE000065	HC	5.05	68.62	0.65	0.05	0.34	0.08	0.30	0.00	0.11	0.25	0.18	99.95	0.00	0.00	0.00	0.00	0.00	0.65	0.10	0.58	2.97	94.86	99.15	5.19	5.35	2.81	5.62			
SEG-DE000066	HC	5.03	69.22	0.58	0.02	0.24	0.01	0.14	0.00	0.01	0.07	0.19	100.04	0.10	0.03	0.58	0.00	0.04	0.28	0.01	0.61	0.00	98.39	100.05	5.21	5.26	3.43	4.34			
SEG-DE000067	HC	5.13	68.78	0.44	0.04	0.30	0.03	0.11	0.00	0.01	0.11	0.18	99.43	0.17	0.07	0.68	0.00	0.04	0.09	0.04	0.58	0.00	98.06	99.75	5.21	5.39	1.47	4.87			
SEG-DE000068	HC	5.05	68.68	0.62	0.01	0.33	0.02	0.19	0.01	0.01	0.18	0.39	99.39	0.01	0.05	0.78	0.00	0.04	0.23	0.02	0.58	0.50	97.16	99.37	5.19	5.31	2.87	5.01			
SEG-DE000072	HC	4.81	69.19	0.36	0.07	0.25	0.00	0.21	0.01	0.09	0.23	0.21	100.20	0.36	0.06	0.40	0.10	0.07	0.00	0.68	0.86	97.47	100.21	5.19	5.39	7.37	10.69				
TAM-DE000046	IF	5.50	21.5	44.49	34.99	0.03	0.37	0.22	0.58	0.01	0.01	0.31	99.90	0.02	0.12	0.81	0.00	0.04	34.58	0.29	0.99	4.34	58.69	99.87	3.87	3.92	44.27	44.97	28.33	27.89	
TAM-DE000047	IF	4.00	2.45	39.49	42.84	0.01	0.51	0.05	0.38	0.01	0.01	0.21	100.29	0.03	0.04	1.25	0.00	0.04	42.23	0.06	0.69	2.36	53.64	100.33	3.67	3.74	33.24	34.52	30.71	29.58	
TAM-DE000048	IF	4.10	2.14	39.29	43.80	0.01	0.26	0.08	0.27	0.00	0.02	0.01	0.25	100.62	0.01	0.03	0.62	0.00	0.07	43.46	0.10	0.80	1.20	54.28	100.57	3.66	3.72	41.50	42.40	22.08	21.61
TAM-DE000049	IF	5.10	2.46	38.31	43.28	0.02	0.64	0.16	0.64	0.05	0.04	0.01	0.20	99.67	0.02	0.08	1.53	0.00	0.11	42.50	0.21	0.63	4.85	49.78	99.70	3.63	3.70	32.32	33.49	40.89	39.46
TAM-DE000050	IF	3.90	2.83	39.27	42.98	0.01	0.41	0.05	0.30	0.00	0.01	0.02	0.27	99.94	0.02	0.04	1.00	0.00	0.04	42.49	0.07	0.86	1.59	53.84	99.95	3.67	3.73	23.01	24.15	49.83	47.47
TAM-DE000052	IF	5.70	2.54	36.64	46.37	0.03	0.18	0.09	0.87	0.00	0.03	0.01	0.23	100.00	0.02	0.09	0.35	0.00	0.09	46.15	0.12	0.73	7.18	45.19	99.92	3.56	3.64	28.68	30.10	53.58	51.06
TAM-DE000053	IF	9.10	2.27	37.77	45.02	0.03	0.18	0.29	0.83	0.00	0.04	0.01	0.44	100.46	0.02	0.09	0.36	0.00	0.13	44.77	0.37	1.41	6.75	46.48	100.38	3.60	3.62	37.12	37.40	61.12	60.65
TAM-DE000055	IF	2.90	3.21	40.10	42.74	0.01	0.13	0.02	0.13	0.00	0.01	0.02	0.24	100.36	0.01	0.02	0.31	0.00	0.04	42.56	0.03	0.78	0.00	56.67	100.42	3.70	3.74	13.36	14.36	71.70	66.69
TAM-DE000078	IGO	12.90	2.09	47.61	26.90	0.12	0.40	0.06	4.37	0.01	0.06	0.01	0.18	100.16	0.01	0.48	0.51	0.00	0.17	26.55	0.08	0.58	41.60	30.09	100.08	3.87	3.91	45.95	46.43	67.44	66.73
TAM-DE000079	IF	9.90	2.17	30.98	52.47	0.05	0.48	0.30	2.64	0.01	0.06	0.01	0.18	100.43	0.01	0.19	1.01	0.00	0.19	51.87	0.39	0.58	24.53	21.65	100.42	3.34	3.39	35.18	36.10	67.68	65.95
TAM-DE000081	IGO	12.90	2.09	42.27	34.77	0.12	0.14	0.05	3.69	0.03	0.05	0.02	0.18	100.43	0.02	0.45	2.40	0.00	0.16	33.95	0.07	0.58	34.89	28.49	100.60	3.68	3.74	43.09	44.04	71.91	70.36
TAM-DE000082	IFR	9.80	2.34	53.84	20.07	0.07	1.60	0.03	1.54	0.04	0.04	0.01	0.35	100.42	0.02	0.26	3.77	0.00	0.11	18.24	0.04	1.14	13.73	63.48	100.78	4.21	4.29	44.34	45.30	57.44	56.22
TAM-DE000089	IAL	8.50	3.09	57.56	7.59	0.09	6.15	0.31	2.76	0.41	0.11	0.02	0.21	99.90	0.03	0.33	15.21	0.00	0.35	0.28	0.40	0.68	25.68	58.53	101.49	4.33	4.56	28.55	30.10	53.58	51.06
TAM-DE000090	IAL	10.20	3.04	59.13	6.88	0.07	5.61	0.09	2.49	0.47	0.10	0.01	0.60	100.32	0.02	0.28	13.91	0.00	0.32	0.20	0.11	1.94	23.05	61.83	101.66	4.40	4.59	31.01	33.87	111.26	101.86
TAM-DE000096	IFR	7.40	2.29	51.72	23.45	0.08	0.50	0.05	0.28	0.00	0.03	0.01	0.62	100.39	0.02	0.29	0.95	0.00	0.08	22.95	0.07	2.00	21.05	52.97	100.40	4.10	4.22	44.45	44.45	41.29	41.10
TAM-DE000097	IAL	9.90	2.33	53.56	17.69	0.04	3.65	0.06	1.97	0.01	0.05	0.02	1.16	99.99	0.03	0.12	9.11	0.00	0.17	13.34	0.08	3.73	17.98	56.57	101.12	4.17	4.27	44.15	45.55	57.91	56.14
TAM-DE000111	HF	19.50	2.37	65.45	1.04	0.08	1.61	1.10	1.58	0.14	0.04	0.06	0.67	99.51	0.00	0.30	2.08	1.00	0.12	1.42	2.15	9.22	83.09	99.38	4.95	5.05	52.19	53.14	109.81	107.84	
TAM-DE000115	HF	6.60	3.34	68.20	0.97	0.03	0.83	0.25	0.71	0.04	0.01	0.11	0.02	100.33	0.00	0.12	1.97	0.00	0.04	0.03											

**Table A1.** Cont.

Sample	Litho	U (%)	$\rho_s$ (g/cm <sup>3</sup> )	Fe (%)	SiO <sub>2</sub> (%)	P (%)	Al <sub>2</sub> O <sub>3</sub> (%)	Mn (%)	LOI (%)	TiO <sub>2</sub> (%)	MgO (%)	CaO (%)	FeO (%)	Clo_Oxi	Ap (%)	Wav (%)	Kln (%)	Gbs (%)	Tlc (%)	Qz (%)	MnO (%)	Mag (%)	Gth (%)	Hem (%)	Clo_Min	$\rho_{\_MNC}$ (g/cm <sup>3</sup> )	$\rho_{\_PYC}$ (g/cm <sup>3</sup> )	$\varphi_{\_MNC}$ (%)	$\varphi_{\_PYC}$ (%)	$\varphi_{s\_MNC}$ (%)	$\varphi_{s\_PYC}$ (%)
CCE-DE000068	IC	3.18	27.78	59.74	0.01	0.19	0.04	0.11	0.00	0.07	0.00	0.18	99.88	0.00	0.04	0.43	0.00	0.21	59.41	0.06	0.58	0.00	39.51	100.25	3.31	3.30	3.64	3.54			
CCE-DE000069	IC	3.56	38.02	44.44	0.00	0.15	0.00	0.13	0.00	0.01	0.00	0.19	99.08	0.00	0.01	0.36	0.00	0.04	44.24	0.00	0.62	0.00	53.79	99.07	3.64	3.63	2.05	1.89			
CCE-DE000070	IC	3.48	37.09	46.06	0.01	0.21	0.00	0.10	0.00	0.04	0.00	0.21	99.44	0.00	0.03	0.50	0.00	0.14	45.73	0.00	0.67	0.00	52.80	99.88	3.61	3.59	3.49	3.03			
CCE-DE000071	IC	3.57	39.59	42.56	0.04	0.18	0.00	0.13	0.00	0.07	0.09	0.22	99.69	0.13	0.06	0.39	0.00	0.23	42.23	0.00	0.70	0.00	56.13	99.89	3.69	3.68	3.23	2.93			
CCE-DE000072	IC	3.67	40.45	41.31	0.03	0.09	0.00	0.09	0.00	0.01	0.08	0.18	99.45	0.13	0.03	0.19	0.00	0.04	41.20	0.00	0.58	0.00	57.75	99.92	3.73	3.71	1.54	1.20			
CMT-FD00154-029	IC	3.36	33.93	50.28	0.01	0.05	0.00	0.17	0.00	0.03	0.02	0.00	99.08	0.03	0.02	0.11	0.00	0.10	50.16	0.00	0.00	0.22	48.32	98.97	3.50	3.56	3.82	5.61			
CMT-FD00154-030	IC	3.24	30.95	55.25	0.01	0.05	0.00	0.15	0.00	0.03	0.01	0.00	99.78	0.02	0.04	0.09	0.00	0.10	55.14	0.00	0.00	0.02	44.25	99.66	3.40	3.43	4.61	5.53			
CMT-FD00154-031	IC	3.31	34.66	49.49	0.01	0.05	0.00	0.36	0.01	0.04	0.01	0.00	99.54	0.02	0.03	0.09	0.00	0.11	49.37	0.00	0.00	0.21	47.63	99.42	3.52	3.56	5.86	7.07			
CMT-FD00154-032	IC	3.21	34.62	49.25	0.02	0.07	0.00	0.32	0.00	0.03	0.02	0.00	99.24	0.03	0.06	0.11	0.00	0.10	49.14	0.00	0.00	1.68	47.99	99.12	3.52	3.56	8.65	9.90			
CMT-FD00154-033	IC	3.35	35.70	48.62	0.02	0.17	0.00	0.18	0.02	0.01	0.02	0.00	100.11	0.03	0.06	0.37	0.00	0.04	48.42	0.00	0.00	0.35	50.75	100.02	3.55	3.57	5.51	6.16			
CMT-FD00154-034	IC	3.60	43.12	37.73	0.01	0.20	0.00	0.40	0.02	0.01	0.01	0.00	100.05	0.01	0.04	0.46	0.00	0.04	37.49	0.00	0.00	2.50	59.41	99.97	3.81	3.82	5.38	5.66			
CMT-FD00154-035	IC	3.02	24.93	64.21	0.01	0.03	0.00	0.06	0.00	0.01	0.01	0.00	99.98	0.02	0.02	0.06	0.00	0.04	64.15	0.00	0.00	0.00	36.43	100.72	3.23	3.24	6.30	6.92			
CMT-FD00154-036	IC	3.35	33.84	50.52	0.01	0.17	0.00	0.13	0.01	0.01	0.01	0.00	99.26	0.02	0.02	0.41	0.00	0.04	50.30	0.00	0.00	0.00	48.49	99.29	3.50	3.51	4.01	4.35			
JGD-FD00001-039	HC	3.86	69.21	0.51	0.01	0.21	0.06	0.28	0.02	0.01	0.06	0.00	100.14	0.00	0.00	0.00	0.00	0.05	0.51	0.08	0.00	2.80	96.45	99.84	5.20	5.21	25.56	25.91			
FNO-DE000077	IC	2.89	42.95	31.18	0.07	0.29	0.84	5.65	0.00	0.03	0.00	0.36	99.76	0.00	0.27	0.46	0.00	0.09	30.91	1.09	1.17	54.34	11.36	99.68	3.69	3.62	21.55	20.12			
JPE-DE000070	HC	3.55	66.59	1.54	0.09	0.70	0.00	0.62	0.04	0.74	0.28	0.56	99.27	0.44	0.13	0.17	0.88	2.31	0.00	0.00	1.80	1.58	91.93	99.25	5.03	5.16	30.43	31.13			
JPE-DE000073	IC	3.19	23.53	65.42	0.01	0.08	0.00	0.16	0.00	0.03	0.00	0.37	99.32	0.00	0.04	0.16	0.00	0.08	65.30	0.00	0.19	0.16	32.27	99.21	3.18	3.24	-0.25	1.45			
MMI-DE000062	IC	3.37	34.89	49.63	0.01	0.04	0.01	0.19	0.00	0.05	0.07	0.20	99.87	0.00	0.00	0.00	0.00	0.00	49.63	0.01	0.64	1.89	47.53	99.70	3.52	3.51	4.12	3.88			
MMI-DE000063	HC	5.16	69.61	0.29	0.01	0.11	0.01	0.14	0.00	0.11	0.03	0.18	100.21	0.05	0.02	0.18	0.05	0.33	0.00	0.01	0.58	0.76	98.25	100.23	5.22	5.21	1.26	0.93			
MMI-DE000067	HC	4.62	64.45	8.14	0.00	0.10	0.01	0.05	0.01	0.01	0.01	0.18	100.45	0.02	0.00	0.25	0.00	0.04	7.99	0.01	0.58	0.00	92.43	101.32	4.87	4.89	4.92	5.48			
SEG-DE000087	IC	3.60	39.78	41.77	0.01	0.07	0.00	0.54	0.00	0.16	0.21	0.32	99.61	0.00	0.00	0.00	0.00	0.00	41.77	0.00	1.03	5.30	51.05	99.16	3.69	3.84	2.32	6.16			

**Table A2.** Original unweathered sample data with lithology, chemical grades, bulk density, moisture, and mineral density (PYC) measurements and calculated mineral proportions, mineral density (CNM), porosity (CNM and PYC), and saturation (CNM and PYC).

Sample	Litho	$\rho_s$ (g/cm <sup>3</sup> )	Fe (%)	SiO <sub>2</sub> (%)	P (%)	Al <sub>2</sub> O <sub>3</sub> (%)	Mn (%)	LOI (%)	TiO <sub>2</sub> (%)	MgO (%)	CaO (%)	FeO (%)	Clo_Oxi	Ap (%)	Ank (%)	Chl (%)	Dol (%)	Cal (%)	Tlc (%)	Qz (%)	MnO (%)	Mag (%)	Hem (%)	Clo_Min	$\rho_{\_MNC}$ (g/cm <sup>3</sup> )	$\rho_{\_PYC}$ (g/cm <sup>3</sup> )	$\varphi_{\_MNC}$ (%)	$\varphi_{\_PYC}$ (%)	
JGD-FD00001-041	IDR	4.05	50.96	20.74	0.03	0.16	0.03	2.49	0.02	0.25	3.08	0.10	99.69	0.15	0.00	0.00	1.13	4.43	0.00	20.74	0.04	0.32	72.52	99.33	4.18	4.16	2.72	3.24	
JGD-FD00001-042	IDSI	3.46	37.72	40.78	0.08	0.01	0.20	2.04	0.01	0.11	2.91	0.10	99.98	0.41	0.00	0.00	0.50	4.08	0.00	40.78	0.02	0.32	53.59	99.69	3.63	3.60	4.06	4.80	
JGD-FD00001-043	IDR	4.40	59.03	0.94	0.16	0.21	0.04	5.85	0.02	0.52	7.90	0.10	100.25	0.84	0.00	0.00	2.37	10.71	0.00	0.94	0.05	0.32	84.06	99.29	4.63	4.66	5.60	5.07	
JGD-FD00001-052	IDSI	3.50	36.46	37.18	0.04	0.01	0.07	4.45	0.00	2.13	3.19	0.10	99.27	0.21	0.00	0.00	9.31	0.00	0.00	37.18	0.09	0.32	51.80	98.90	3.64	3.64	3.99	3.51	
JGD-FD00004-043	HDO	4.42	64.92	5.82	0.27	1.08	0.01	0.98	0.09	1.19	0.94	0.10	103.54	1.46	0.00	0.00	0.40	0.00	0.00	3.46	3.63	0.01	0.32	92.48	101.77	4.88	4.70	5.92	9.27
JGD-FD00004-049	HDO	4.36	60.37	0.85	0.09	0.11	0.06	4.09	0.01	0.15	8.64	0.10	100.44	0.46	0.00	0.00	0.70	8.53	0.00	0.85	0.07	0.32	85.98	96.92	4.78	4.55	4.21	8.80	
JGD-FD00004-053	HDO	4.34	61.24	0.64	0.16	0.24	0.04	3.56	0.02	0.28	6.57	0.10	99.27	0.84	0.00	0.00	1.27	6.68	0.00	0.64	0.05	0.32	87.21	97.01	4.84	4.70	7.77	10.28	
JGD-FD00004-055	HDO	4.46	65.17	0.57	0.12	0.07	0.04	1.58	0.02	0.15	4.68	0.10	100.55	0.62	0.00	0.00	0.66	2.85	0.00	0.57	0.05	0.32	92.85	97.92	5.04	4.82	7.43	11.57	
JGD-FD00004-057	IDR	4.28	57.73	0.60	0.07	0.21	0.09	6.29	0.01	0.33	9.86	0.10	100.11	0.40	0.00	0.00	1.51	12.66	0.00	0.60	0.11	0.32	82.20	97.79	4.60	4.53	5.55	6.95	
JGD-FD00004-063	IDR	3.84	45.98	0.54	0.09	0.13	0.30	14.57	0.00	4.55	13.28	0.10	99.39	0.48	0.00	0.00	20.80	10.54	0.00	0.54	0.38	0.32	65.40	98.46	4.09	4.09	6.25	6.10	
JGD-FD00005-039	IDR	4.00	51.94	0.99	0.11	0.15	0.12	10.13	0.01	5.38	8.66	0.10	99.97	0.59	0.00	0.00	21.20	0.00	0.00	0.99	0.15	0.32	73.92	97.18	4.39	4.24	5.60	8.77	
JGD-FD00005-040	IDR	3.96	45.41	2.42	0.07	0.87	0.13	13.82	0.05	2.52	7.22	10.09	0.10	99.72	0.37	0.00	0.00	28.94	0.00	0.00	2.41	0.17	0.32	64.59	96.82	4.11	4.00	1.02	3.65
JGD-FD00005-041	DO	2.85	17.53	3.60	0.04																								

**Table A2.** Cont.

Sample	Litho	$\rho_s$ (g/cm <sup>3</sup> )	Fe (%)	SiO <sub>2</sub> (%)	P (%)	Al <sub>2</sub> O <sub>3</sub> (%)	Mn (%)	LOI	TiO <sub>2</sub> (%)	MgO (%)	CaO	FeO (%)	Clo_Oxi	Ap (%)	Ank (%)	Chl	Dol (%)	Cal (%)	Tlc	Qz (%)	MnO (%)	Mag	Hem	Clo_Min	$\rho_{MNC}$ (g/cm <sup>3</sup> )	$\rho_{PYC}$ (g/cm <sup>3</sup> )	$\varphi_{MNC}$ (%)	$\varphi_{PYC}$ (%)
JGD-FD00009-046	IDR	4.25	55.91	2.31	0.09	0.52	0.06	6.74	0.03	0.81	9.59	0.10	100.24	0.49	0.00	0.00	3.71	11.28	0.00	2.31	0.08	0.32	79.60	97.80	4.51	4.41	3.75	5.81
JGD-FD00013-034	DO	2.86	3.28	1.86	0.03	0.77	0.77	42.17	0.05	20.44	29.21	0.10	100.25	0.17	0.00	0.00	88.34	0.00	0.00	1.85	0.99	0.32	4.35	96.04	2.92	2.98	4.01	2.04
JGD-FD00013-036	IDO	3.76	42.78	0.84	0.06	0.20	0.25	18.07	0.01	7.39	12.58	0.10	100.70	0.31	0.00	0.00	33.81	3.80	0.00	0.84	0.32	0.32	60.82	100.22	3.95	3.94	4.53	4.73
JGD-FD00013-037	DO	2.83	4.74	0.80	0.01	0.34	0.37	43.47	0.00	20.68	27.93	0.10	100.49	0.05	0.00	0.00	91.07	0.00	0.00	0.79	0.48	0.32	6.44	99.17	2.95	2.95	4.02	3.90
JGD-FD00013-038	IDO	3.32	26.30	0.75	0.02	0.15	0.47	29.09	0.00	11.89	19.46	0.10	99.59	0.11	0.00	0.00	54.39	5.11	0.00	0.75	0.60	0.32	37.27	98.55	3.45	3.46	4.26	3.90
JGD-FD00013-041	IDO	3.42	31.97	0.84	0.10	0.26	0.76	24.67	0.01	8.77	18.77	0.10	100.21	0.51	0.00	0.00	40.11	11.21	0.00	0.84	0.98	0.32	45.38	99.35	3.60	3.59	4.89	5.18
JGD-FD00013-048	IDO	4.00	48.26	0.80	0.03	0.01	0.19	13.57	0.00	3.34	13.06	0.10	100.07	0.14	0.00	0.00	15.28	14.27	0.00	0.80	0.24	0.32	68.66	99.71	4.13	4.14	3.43	3.25
JGD-FD00013-049	IDSI	3.53	38.07	33.61	0.05	0.21	0.15	5.71	0.01	2.74	3.82	0.10	100.83	0.25	0.00	0.00	11.95	0.00	0.00	33.60	0.20	0.32	54.09	100.43	3.67	3.68	4.02	3.81
JGD-FD00013-051	IDSI	3.19	27.91	43.57	0.05	0.04	0.11	7.56	0.00	3.24	5.26	0.10	99.81	0.24	0.00	0.00	14.82	1.10	0.00	43.57	0.14	0.32	39.57	99.76	3.35	3.35	4.94	5.07
JGD-FD00014-058	IDO	3.83	43.48	1.17	0.10	0.22	0.12	16.11	0.01	1.37	19.19	0.10	100.60	0.54	0.00	0.00	6.24	29.83	0.00	1.17	0.15	0.32	61.83	100.08	3.91	3.91	2.00	1.92
JGD-FD00014-059	HDO	4.56	61.96	1.80	0.10	0.39	0.06	4.42	0.03	0.20	5.10	0.10	100.82	0.52	0.00	0.00	0.91	8.08	0.00	1.80	0.07	0.32	88.26	99.96	4.76	4.73	3.68	4.30
JGD-FD00014-063	IDO	3.28	23.89	2.69	0.06	1.22	0.46	29.43	0.08	13.09	18.99	0.10	100.39	0.34	0.00	0.00	59.89	1.04	0.00	2.69	0.60	0.32	33.82	98.70	3.39	3.39	3.27	3.32
JGD-FD00015-062	IDR	4.05	56.96	1.30	0.08	0.54	0.06	7.47	0.05	0.88	8.62	0.10	100.54	0.41	0.00	0.00	4.04	12.60	0.00	1.30	0.07	0.32	81.10	99.83	4.50	4.51	10.18	10.08
JGD-FD00022-024	IDSI	3.07	22.76	34.70	0.05	0.26	0.16	14.96	0.01	6.53	10.01	0.10	99.32	0.25	0.00	0.00	29.87	1.39	0.00	34.70	0.21	0.32	32.21	98.96	3.26	3.29	6.77	5.85
JGD-FD00022-028	IDSI	3.38	34.58	40.70	0.08	0.20	0.20	3.62	0.01	2.26	3.16	0.10	99.83	0.41	0.00	0.00	7.58	0.00	0.00	40.70	0.26	0.32	49.11	98.37	3.56	3.54	4.42	5.18
JGD-FD00035-035	IDR	3.92	48.54	0.67	0.13	0.03	0.08	12.75	0.00	1.05	15.80	0.10	100.10	0.69	0.00	0.00	4.78	23.78	0.00	0.67	0.11	0.32	69.06	99.42	4.12	4.15	5.68	5.02
JGD-FD00035-036	IDSI	3.24	38.56	39.97	0.11	0.10	0.02	1.68	0.01	0.14	2.54	0.10	99.83	0.60	0.00	0.00	0.63	3.12	0.00	39.97	0.02	0.32	54.80	99.45	3.67	3.67	11.78	11.64
JGD-FD00035-037	HDO	4.52	64.94	2.21	0.12	0.29	0.07	2.07	0.03	0.12	2.82	0.10	100.74	0.64	0.00	0.00	0.53	4.10	0.00	2.21	0.09	0.32	92.50	100.40	4.92	4.94	8.43	8.15
JGD-FD00035-038	IDO	4.36	59.34	1.04	0.13	0.11	0.06	5.73	0.02	0.22	8.03	0.10	100.33	0.68	0.00	0.00	0.98	11.93	0.00	1.04	0.08	0.32	84.50	99.53	4.63	4.66	6.37	5.82
JGD-FD00035-039	HDO	4.45	60.48	0.62	0.16	0.24	0.06	4.95	0.02	0.51	7.50	0.10	100.74	0.88	0.00	0.00	2.32	8.69	0.00	0.62	0.07	0.32	86.14	99.04	4.72	4.67	4.83	5.81
JGD-FD00035-042	IDO	4.01	53.02	9.96	0.08	0.09	0.04	5.50	0.01	0.15	8.28	0.10	100.03	0.44	0.00	0.00	0.69	11.75	0.00	9.96	0.06	0.32	75.47	98.68	4.31	4.31	6.93	7.03
JGD-FD00035-044	IDSI	3.25	28.42	38.45	0.04	0.04	0.11	9.72	0.00	4.47	7.08	0.10	100.63	0.23	0.00	0.00	20.36	0.00	0.00	38.45	0.14	0.32	40.30	99.79	3.39	3.38	3.77	3.91
JGD-FD00035-046	IDSI	3.28	32.81	38.92	0.10	0.07	0.06	6.03	0.00	2.95	5.03	0.10	100.21	0.52	0.00	0.00	12.60	0.00	0.00	38.92	0.08	0.32	46.57	99.02	3.51	3.48	5.89	6.62
JGD-FD00035-047	IDSI	3.16	29.31	32.43	0.06	0.07	0.06	10.35	0.00	2.78	11.98	0.10	99.71	0.31	0.00	0.00	12.71	9.74	0.00	32.43	0.08	0.32	41.56	97.14	3.43	3.42	7.78	7.83
JGD-FD00035-048	IDSI	3.41	35.43	39.60	0.03	0.04	0.10	3.34	0.00	2.48	3.48	0.10	99.77	0.14	0.00	0.00	6.98	0.00	0.00	39.60	0.13	0.32	50.32	97.49	3.60	3.54	3.62	5.29
JGD-FD00035-049	IDO	3.12	26.04	49.87	0.04	0.03	0.07	5.61	0.00	2.01	5.23	0.10	100.17	0.21	0.00	0.00	9.21	2.75	0.00	49.87	0.10	0.32	36.90	99.35	3.29	3.27	4.63	5.06
JGD-FD00036-068	HDO	4.78	67.65	2.91	0.07	0.04	0.02	1.79	0.02	0.22	2.09	0.10	103.95	0.36	0.00	0.00	1.01	2.83	0.00	2.91	0.02	0.32	96.38	103.83	4.95	4.92	2.77	3.27
JGD-FD00036-074	IDR	4.38	58.65	0.80	0.04	0.13	0.05	6.22	0.01	0.23	9.42	0.10	100.80	0.19	0.00	0.00	1.07	12.98	0.00	0.80	0.06	0.32	83.52	98.93	4.61	4.47	2.09	5.08
JGD-FD00036-076	IDR	4.45	58.90	1.53	0.10	0.33	0.05	5.50	0.03	0.49	7.79	0.10	100.18	0.55	0.00	0.00	2.25	10.05	0.00	1.53	0.07	0.32	83.88	98.64	4.64	4.49	0.92	4.22
ABO-FD00011-066	DO	2.73	4.46	23.58	0.01	0.49	0.64	33.77	0.01	13.35	22.61	3.89	102.80	0.06	0.00	0.00	61.07	7.14	0.00	23.58	0.82	6.16	0.00	98.84	2.88	2.86	4.79	5.34
SEG-DE000075	DO	2.71	1.17	0.57	0.02	0.18	0.24	46.11	0.00	23.50	31.43	0.33	103.77	0.09	0.00	0.00	96.60	0.00	0.00	0.56	0.30	1.05	0.58	99.19	2.87	2.96	8.68	5.84
SEG-DE000077	DO	2.78	1.43	0.27	0.01	0.10	1.09	45.52	0.00	22.60	31.10	0.32	103.02	0.05	0.00	0.00	95.37	0.00	0.00	0.26	1.40	1.02	0.99	99.10	2.89	2.97	6.43	3.86
SEG-DE000080	DO	2.81	5.20	1.33	0.04	0.61	0.63	42.38	0.02	21.38	28.62	1.04	102.54	0.20	0.00	0.00	88.78	0.00	0.00	1.33	0.81	3.34	3.97	98.44	2.96	3.03	7.10	4.84
SEG-DE000085	DO	2.98	12.79	1.48	0.02	0.17	0.43	37.34	0.00	17.50	25.25	2.02	100.42	0.13	0.00	0.00	78.22	0.00	0.00	1.48	0.56	6.52	11.54	98.45	3.11	3.20	6.78	4.17
SEG-DE000086	IDO	3.16	24.34	12.54	0.03	0.23	0.29	24.47	0.00	11.52	16.07	0.81	99.98	0.16	0.00	0.00	51.25	0.00	0.00	12.54	0.38	2.61	32.11	99.04	3.36	3.48	9.32	6.15

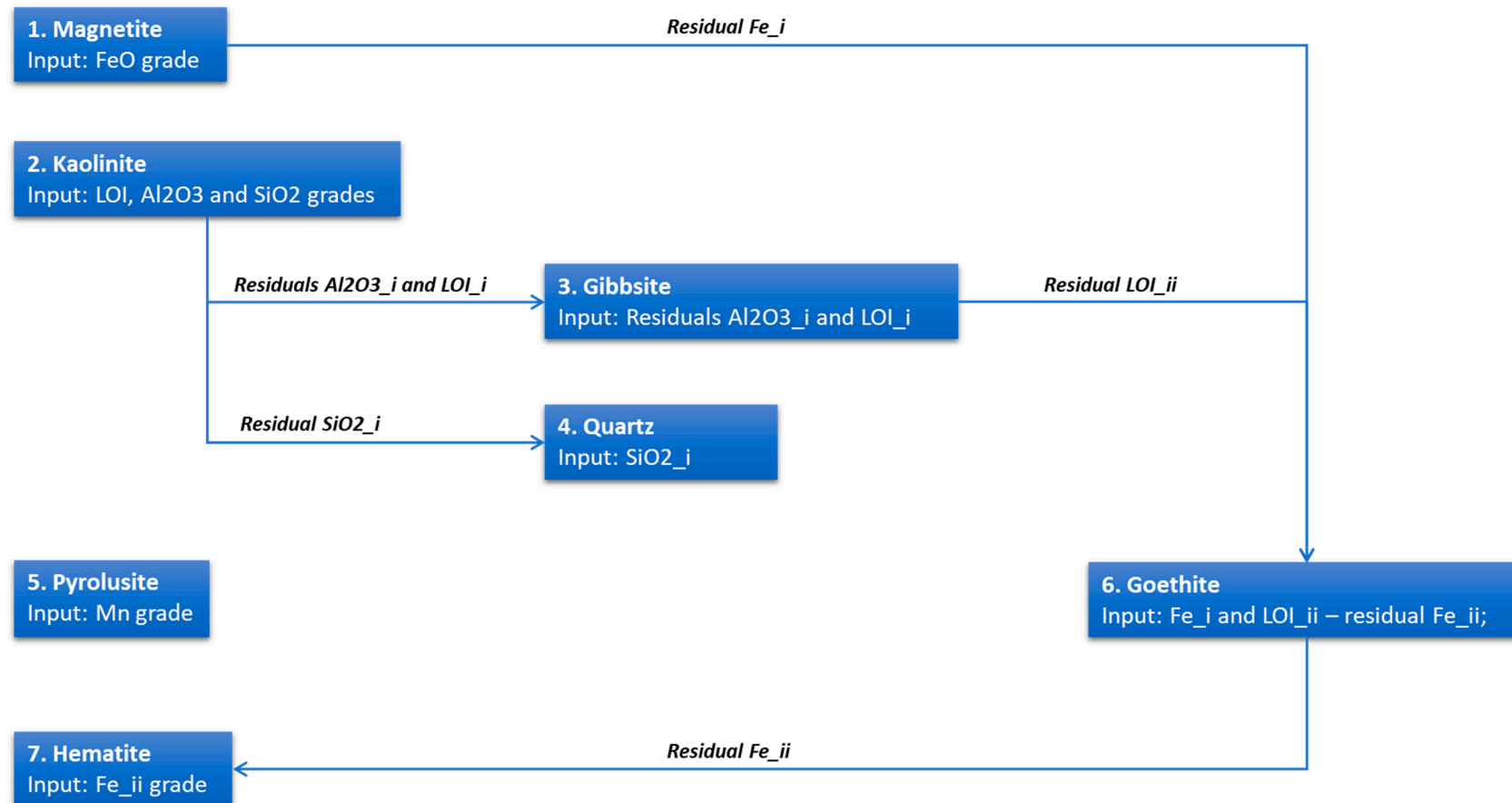


**Figure A1.** Flowchart of algorithm for weathered samples.

## References

1. Dorr, J.v.N. Supergene iron ores of Minas Gerais, Brazil. *Econ. Geol.* **1965**, *59*, 12041–12240. [[CrossRef](#)]
2. Ribeiro, D.T. Enriquecimento Supergênico de Formações Ferríferas Bandadas: Estruturas de Colapso e Desordem. Ph.D. Thesis, Universidade Federal do Estado do Rio de Janeiro, Instituto de Geociências, Programa de Pós-Graduação em Geologia, Rio de Janeiro, Brazil, 2004; 123p.
3. Ribeiro, D.T.; Carvalho, R.M. Simulation of weathered iron ore facies: Integrating leaching concepts and geostatistical model. In *Geostatistics Rio*; Armstrong, M., Bettini, C., Champigny, N., Galli, A., Remacre, A., Eds.; Kluwer Academic: Dordrecht, The Netherlands; pp. 111–115.
4. Voicu, G.; Bardoux, M.; Voicu, D. Mineralogical norm calculations applied to tropical weathering profiles. *Mineral. Mag.* **1997**, *61*, 185–196. [[CrossRef](#)]
5. Motta, E.G.M. Definição de Domínios Mineralógicos em Minério de Ferro Utilizando Krigagem de Indicadores. Master's Thesis, Universidade Federal do Rio Grande do Sul, Escola de Engenharia, Programa de Pós-Graduação em Engenharia de Minas, Metalurgia e de Materiais (PPG3EM), Porto Alegre, Brazil, 2014; 220p.
6. Spier, C.A.; de Oliveira, S.M.B.; Rosière, C.A.; Ardisson, J.D. Mineralogy and trace-element geochemistry of the high-grade iron ores of the Águas Claras Mine and comparison with the Capão Xavier and Tamanduá iron ore deposits, Quadrilátero Ferrífero, Brazil. *Miner. Depos.* **2008**, *43*, 229–254. [[CrossRef](#)]
7. Motta, E.G.M.; Santos, P.A.; Ribeiro, D.T.; Cunha Filho, E.M.C. Incorporating mineralogical and density parameters in ferrous resource evaluation using Mineralogical Norm Calculation—MNC. In Proceedings of the 24th World Mining Congress, Rio de Janeiro, Brazil, 18–21 October 2016; Volume 13, pp. 209–221.
8. Spier, C.A.; Levett, A.; Ardisson, J.D. Geochemistry and genesis of the ferruginous duricrust (canga) developed within the lateritic profile of banded iron formations (BIFs) and BIFs-derived iron ores at the Águas Claras mine, Quadrilátero Ferrífero, Minas Gerais, Brazil. *Miner. Depos.* **2018**. [[CrossRef](#)]
9. Rosière, C.A.; Spier, C.A.; Rios, F.J.; Suckau, V.E. The itabirites of the Quadrilatero Ferrifero and related high-grade iron ore deposits: An overview. In *Banded Iron Formation-Related High-Grade Iron Ore*; Hagemann, S., Rosiere, C., Gutzmer, J., Beukes, N.J., Eds.; Reviews in Economic Geology; Society of Economic Geologists: Littleton, CO, USA, 2008; Volume 15, pp. 223–254.
10. Guimarães, D. Notas a margem da crítica. *Inst. Tecn. Indust. Avulso* **1953**, *16*, 3–39.
11. Dorr, J.v.N.; Barbosa, A.L.M. Geology and ore deposits of the Itabira district, Minas Gerais, Brazil. *U.S. Geol. Surv. Prof. Pap.* **1963**, *341-C*, 110.
12. Park, C.F., Jr. The origin of the hard hematite in Quadrilátero Ferrífero, Minas Gerais, Brazil. *Econ. Geol.* **1959**, *54*, 573–587. [[CrossRef](#)]
13. Guild, P.W. Geology and mineral resources of the Congonhas District, Minas Gerais. *U.S. Geol. Surv. Prof. Pap.* **1957**, *290*, 90.
14. Pomerene, J.B. Geology and ore deposits of the Belo Horizonte, Ibirité and Macacos Quadrangles, Minas Gerais, Brazil. *U.S. Geol. Surv. Prof. Pap.* **1964**, *341-D*, 84.
15. Dorr, J.v.N. Nature and origin of the high-grade hematite ores of Minas Gerais, Brazil. *Econ. Geol.* **1965**, *60*, 1–46. [[CrossRef](#)]
16. Barbour, A.P. Textura, abrandamento e distribuição do fósforo no minério de ferro de Itabira, MG. Ph.D. Thesis, Instituto de Geociências, Universidade de São Paulo, São Paulo, Brazil, 1968.
17. Varajão, C.A.C.; Ramanaidou, E.; Colin, F.; Nahon, D. Gênese dos corpos de Hematita compacta (“Hard hematite ores”): Metassomatismo, sedimentação ou alteração supergênica? *Rem. Ver. Esc. Minas Ouro Preto* **1997**, *50*, 40–43.
18. Varajão, C.A.C.; Ramanaidou, E.; Colin, F.; Nahon, D. Martitização: Alteração supergênica da magnetita. *Rem. Rev. Esc. Minas Ouro Preto* **1996**, *49*, 18–19.
19. Morris, R.C. A textural and mineralogical study of the relationship of iron ore to banded iron-formation in the Hamersley iron province of Western Australia. *Econ. Geol.* **1980**, *75*, 184–209. [[CrossRef](#)]
20. Morris, R.C. Genesis of iron ore in iron-formation by supergene and supergene-metamorphic processes—A conceptual model. In *Handbook of Stratabound and Stratiform Ore Deposits*; Wolf, K.H., Ed.; Elsevier: Amsterdam, The Netherland, 1985; Volume 13, pp. 73–235.
21. Lima, M.R.; Salard-Cheboldaeff, M. Palynologie des bassins de Gandarela et Fonseca (Eocene de L'etat de Minas Gerais, Bresil). *Bol. Inst. Geociências Univ. São Paulo* **1981**, *12*, 33–54. [[CrossRef](#)]
22. Maizatto, J.R. Análise Bioestratigráfica, Paleoecológica e Sedimentológica das Bacias Terciárias do Gandarela e Fonseca Quadrilátero Ferrífero com Base nos Aspectos Palinológicos e Sedimentares. Ph.D. Thesis, Universidade Federal de Ouro Preto, Ouro Preto, Brazil, 2001.
23. Ribeiro, D.T.; Zavaglia, G. Bacias Terciárias e enriquecimento de minério de ferro, An. IX Simpósio de Geologia de Minas Gerais, Ouro Preto. *Soc. Bras. Geol.* **1998**, *14*, 139–140.
24. Viel, R.S.; Moreira, P.C.H.; Alkimim, F.F. Faciologia da Formação Cauê e Gênese do Minério de ferro Friável de Águas Claras, Serra do Curral–M.G. *An. Simpósio Sist. Depos. Pré-Cambr. Ouro Preto* **1987**, *137–147*.
25. Spier, C.A.; Vasconcelos, P.M.; Oliveira, S.M.B.  $^{40}\text{Ar}/^{39}\text{Ar}$  geochronological constraints on the evolution of lateritic iron deposits in the Quadrilátero Ferrífero, Minas Gerais, Brazil. *Chem. Geol.* **2006**, *234*, 79–104. [[CrossRef](#)]

26. Santos, P.A. *Estudo de Densidade de Rochas e Comparação de Técnicas de Medição, na Região do Quadrilátero Ferrífero*; Monografia (Graduação)-Instituto Superior de Ensino de Itabira: Itabira, MG, Brazil, 2006; 58p.
27. Santos, P.A. Variação de densidade das rochas na região do Quadrilátero Ferrífero. In *Simpósio Brasileiro de Minério de Ferro*, 8th ed.; Annals: Salvador, Brazil, 2007; pp. 746–754.
28. Braga, D.M. Técnicas de análises de densidade e porosidade de minério de ferro por Cálculo Normativo Mineralógico, Microtomografia Computadorizada, Permoporosimetria e Picnometria Clássica: Um estudo comparativo entre os métodos. Master's Thesis, Universidade Federal de Minas Gerais, Belo Horizonte, Brazil, 2019; 277p.